

1 **Dynamic and timing properties of new aerosol particle** 2 **formation and consecutive growth events**

3 Imre Salma and Zoltán Németh

4 Institute of Chemistry, Eötvös University, H-1518 Budapest, P.O. Box 32, Hungary

5 Correspondence to: Imre Salma (salma@chem.elte.hu)

6 **Abstract.** Dynamic properties, i.e. particle formation rate J_6 and particle diameter growth rate
7 GR_{10} , and timing properties, i.e. starting time (t_1) and duration time interval (Δt) of 247
8 quantifiable atmospheric NPF and growth events identified in the city centre and near-city
9 background of Budapest over 6 full measurement years together with related gas-phase H_2SO_4
10 proxy, condensation sink (CS) of vapours, basic meteorological data and concentrations of
11 criteria pollutant gases were derived, evaluated, discussed and interpreted. In the city centre,
12 nucleation ordinarily starts at 09:15 UTC+1, and it is maintained for approximately 3 h. The
13 NPF and growth events produce 4.6 aerosol particles with a diameter of 6 nm in 1 cm³ of air in
14 1 s, and cause the particles with a diameter of 10 nm to grow with a typical rate of 7.3 nm h⁻¹.
15 Nucleation starts approximately 1 h earlier in the near-city background, it shows substantially
16 smaller J_6 (with a median of 2.0 cm⁻³ s⁻¹) and GR_{10} values (with a median of 5.0 nm h⁻¹), while
17 the duration of nucleation is similar to that in the centre. Monthly distributions of the dynamic
18 properties and daily maximum H_2SO_4 proxy do not follow the mean monthly pattern of the
19 event occurrence frequency. The factors that control the event occurrence and that govern the
20 intensity of particle formation and growth are not directly linked. New particle formation and
21 growth processes advance in a different manner in the city and its close environment. This could
22 likely be related to diversities in atmospheric composition, chemistry and physics. Monthly
23 distributions and relationships among the properties mentioned provided indirect evidence that
24 chemical species other than H_2SO_4 largely influence the particle growth and possibly
25 atmospheric NPF process as well. The J_6 , GR_{10} and Δt can be described by log-normal
26 distribution function. Most of the extreme dynamic properties could not be explained by
27 available single or compound variables. Approximately 40% of the NPF and growth events
28 exhibited broad beginning, which can be an urban feature. For doublets, the later onset
29 frequently shows more intensive particle formation and growth than the first onset by a typical
30 factor of approximately 1.5. The first event is attributed to regional type, while the second event,
31 superimposed on the first, is often associated with sub-regional, thus urban NPF and growth
32 process.

33

34 **1 Introduction**

35

36 Molecules and molecular fragments in the air collide randomly and can form electrically neutral
37 or charged clusters. Most clusters decompose shortly. Chemical stabilising interactions among
38 certain components within a cluster can enhance its lifetime, during which it can grow further
39 by additional molecular collisions through some distinguishable size regimes (Kulmala et al.,
40 2014). If the diameter of these clusters reaches a critical value of 1.5 ± 0.3 nm (Kulmala et al.,
41 2013), they become thermodynamically stable, and their further growth turns into a spontaneous
42 process. Supersaturation is a necessary atmospheric condition for this principal transformation.
43 It is essentially a phase transition, which takes place in a dispersed manner in the atmosphere,
44 so it generates an aerosol system. The newly formed particles grow further by condensation to
45 larger sizes in most cases due to the existing supersaturation. Photochemical oxidation products
46 such as H_2SO_4 (Sipilä et al., 2010), extremely low-volatile organic compounds (ELVOCs, Ehn
47 et al., 2014; Jokinen et al., 2015) and highly oxygenated molecules (HOMs, Bianchi et al., 2016;
48 Kirkby et al., 2016; Tröstl et al., 2016) together with H_2O vapour, NH_3 (Kirkby et al., 2011),
49 amines (Almeida et al., 2013), other oxidation products of volatile organic compounds (VOCs;
50 Metzger et al., 2010; Schobesberger et al., 2013; Riccobono et al., 2014) and some inhibiting
51 chemical species (e.g. isoprene or NO_2 ; Kiendler-Scharr et al., 2009; Kerminen et al., 2018)
52 can play an important role in both the particle formation and growth. The VOCs include
53 compounds of both anthropogenic and biogenic origin, mainly isoprenoids such as α -pinene
54 (Kirkby et al., 2016). In some specific coastal regions, iodine oxides produced from marine
55 biota are involved (O'Dowd et al., 2002). Atmospheric concentration of these key compounds
56 at a level that is smaller by 12–14 orders of magnitude than the concentration of air molecules
57 is already sufficient for the phenomenon (Kulmala et al., 2014). Relative importance of the
58 organics increases with particle size (Riipinen et al., 2011; Ehn et al., 2014), and their
59 supersaturation is maintained by fast gas-phase autooxidation reactions of VOCs (Crouse et
60 al., 2013). The overall phenomenon is ordinarily confined in time for 1 day or so, and, therefore,
61 it can be regarded as an event in time, and is referred as new aerosol particle formation (NPF)
62 and consecutive particle diameter growth event.

63

64 Such events appear to take place almost everywhere in the world and anytime (Kulmala et al.,
65 2004; Kerminen et al., 2018; Nieminen et al., 2018). Their occurrence frequency and, more
66 importantly, their contribution to particle number concentrations were found to be substantial

67 or determinant in the global troposphere (Spracklen et al., 2006; Kulmala et al., 2014).
68 Moreover, their contribution to the number of cloud condensation nuclei (CCN) can be 50% or
69 even more (Makkonen et al., 2009; Merikanto et al., 2009; Sihto et al., 2011), which links the
70 events to climate system, and emphasizes their global relevance (Kerminen et al., 2012;
71 Makkonen et al., 2012; Carslaw et al., 2013; Gordon et al., 2016). New particle formation and
72 growth events were proved to be common in polluted air of large cities as well with a typical
73 relative occurrence frequency between 10% and 30% (Woo et al., 2001; Baltensperger et al.,
74 2002; Alam, et al., 2003; Wehner et al., 2004; Salma et al., 2011; Dall'Osto et al., 2013; Xiao
75 et al., 2015; Zhang et al., 2015; Kulmala et al., 2017, Nieminen et al., 2018). The coupling and
76 relationships between regional and urban (sub-regional) NPF were demonstrated at least under
77 favourable orographic conditions (Salma et al., 2016b). New particle formation can increase
78 the existing particle number concentrations in city centres by a factor of approximately 2 on
79 nucleation days, while it can produce 13–28% of ultrafine (UF) particles as a lower estimate on
80 a longer (e.g. annual) time scale (Salma et al., 2017). Particle concentrations from NPF are also
81 important when compared to (primary) particles emitted by their dominant source in cities,
82 namely by road vehicles with internal combustion engines (Paasonen et al., 2016). These results
83 jointly suggest that particles from NPF and growth events in cities can influence not only the
84 urban climate but can contribute to the public's excess health risk from particle number
85 exposures (Oberdörster et al., 2005; Braakhuis et al., 2014; Salma et al., 2015), and,
86 furthermore, could be linked to the role of human actions in all these effects.

87
88 Despite these potentials, conclusive interpretation of the data obtained, and results derived
89 specifically for cities remained hindered so far. Several-year long, semi-continuous, critically
90 evaluated, complex and coherent data sets are required for this purpose, which have been
91 generating gradually. As part of this international progress, investigations dedicated to urban
92 NPF and growth events in Budapest have been going on since November 2008. Measurements
93 for 5 full years were realised in the city centre at a fixed location, 1 full year was devoted to
94 measurements in a near-city background environment, and some other measurements were
95 accomplished in different urban microenvironments for time intervals of a few months. The
96 main objectives of this study are to determine, present and analyse the dynamic properties, i.e.
97 particle formation rate and particle diameter growth rate, timing properties, i.e. starting time
98 and duration time interval of nucleation process of NPF and growth events together with the
99 major sources and sink of condensing vapours, basic meteorological data and criteria pollutant
100 gases for 6 years, to investigate and interpret their relationships, to discuss their monthly

101 distributions, to evaluate and detect some of their features specific for urban atmospheric
102 environments, and to demonstrate some specific urban influence on the calculation of the
103 properties. These quantities and relationships are of basic importance in many atmospheric
104 processes for several reasons. Our goals are in line with the research needs for global
105 atmospheric nucleation studies (Kerminen et al., 2018; Nieminen et al., 2018).

106

107 **2 Experimental methods**

108

109 The measurements took place at two urban locations in Budapest, Hungary. Most measurements
110 were realised at the Budapest platform for Aerosol Research and Training (BpART) facility (N
111 47° 28' 29.9", E 19° 3' 44.6", 115 m above mean sea level (a.s.l.; Salma et al., 2016a). This site
112 represents a well-mixed, average atmospheric environment for the city centre. The other
113 location was situated at the NW border of Budapest in a wooded area of the Konkoly
114 Astronomical Observatory of the Hungarian Academy of Sciences (N 47° 30' 00.0", E 18° 57'
115 46.8", 478 m a.s.l.). This site characterises the air masses entering the city since the prevailing
116 wind direction in the area is NW. The measurements were accomplished for 6 full-year long
117 time intervals, i.e. from 03–11–2008 to 02–11–2009, from 19–01–2012 to 18–01–2013, from
118 13–11–2013 to 12–11–2014, from 13–11–2014 to 12–11–2015, from 13–11–2015 to 12–11–
119 2016 and from 28–01–2017 to 27–01–2018. In the measurement year 2012–2013, the
120 instruments were set up in the near-city background, while in all other years, they were installed
121 in the city centre. Local time (LT=UTC+1 or daylight-saving time, UTC+2) was chosen as the
122 time base of the data unless otherwise indicated because it had been observed in earlier
123 investigations that the daily activity time pattern of inhabitants substantially influences many
124 atmospheric processes in cities (Salma et al., 2014; Sun et al. 2019).

125

126 The main measuring system was a flow-switching type differential mobility particle sizer
127 (DMPS). It consists of a radioactive (⁶⁰Ni) bipolar charger, a Nafion semi-permeable membrane
128 dryer, a 28-cm long Vienna-type differential mobility analyser and a butanol-based
129 condensation particle counter (TSI, model CPC3775). The sample flow was 2.0 L min⁻¹ in the
130 high-flow mode, and 0.31 L min⁻¹ in the low-flow mode with sheath air flow rates 10 times
131 larger than for the sample flows. The DMPS measures particle number concentrations in an
132 electrical mobility diameter range from 6 to 1000 nm in the dry state of particles (with a relative
133 humidity of RH<30%) in 30 channels, which finally yields 27 channels after averaging 3
134 overlapping channels when joining the data for the 2 flow modes. The time resolution of the

135 measurements was approximately 10 min till 18–01–2013, and 8 min from 13–11–2013 (after
136 a planned update of the DMPS system). There was no upper size cut-off inlet applied to the
137 sampling line, and a weather shield and insect net were only attached. The sampling inlets were
138 identical at both locations except for the height of the installation above the ground, which was
139 12.5 m in the city centre and approximately 1.7 m in the near-city background. The
140 measurements were performed according to the international technical standard (Wiedensohler
141 et al., 2012). The availability of the DMPS data over 1-year long time intervals are summarised
142 in Table 1.

143

144 Synoptic meteorological data for air temperature (T), RH, wind speed (WS) and wind direction
145 (WD) were obtained from a measurement station of the Hungarian Meteorological Service
146 (HMS, station no. 12843) by standardised methods with a time resolution of 1 h. Global solar
147 radiation (GRad) data were measured by the HMS at a distance of 10 km in E direction with a
148 time resolution of 1 h. Meteorological data were available in >90% of the possible cases in each
149 year. Concentrations of SO₂, O₃, NO_x and CO were obtained from measurement stations of the
150 National Air Quality Network in Budapest (in a distance of 4.5 km from the urban site, and of
151 6.9 km from the near-city background site) located in the upwind prevailing direction from the
152 measurement sites. They are measured by UV fluorescence (Ysselbach 43C), UV absorption
153 (Ysselbach 49C), chemiluminescence (Thermo 42C) and IR absorption methods (Thermo 48i),
154 respectively with a time resolution of 1 h. The concentration data were available in >85% of
155 the yearly time intervals, and >98% of them were above the limit of determinations (LOD). It
156 is worth mentioning that the LOD of the SO₂ analyser was approximately 0.2 µg m⁻³, and that
157 the hourly average SO₂ concentration in the Budapest area is ordinarily distributed without
158 larger spatial gradients (Salma et al., 2011). For the present study, this was proved by evaluating
159 the concentration ratios from 2 different municipal stations which are in the closest distance
160 from the BpART facility in 2 different directions with an angle of 60° between them. The mean
161 SO₂ concentration ratio and standard deviation (SD) for the 2 stations were 81±20% over the
162 5-year long measurement time interval. The assumption can also be justified indirectly by a
163 conclusion on the monthly distribution of SO₂ concentration in Sect. 4.2.

164

165 **3 Data treatment**

166

167 The measured DMPS data were evaluated according to the procedure protocol recommended
168 by Kulmala et al. (2012) with some refinements that are related to urban features (see Sect. 3.1).

169 Particle number concentrations in the diameter ranges from 6 to 1000 nm (N), from 6 to 25 nm
170 (N_{6-25}), from 6 to 100 nm (N_{6-100} or UF particles) and from 100 to 1000 nm ($N_{100-1000}$) were
171 calculated from the measured and inverted DMPS concentrations. Particle number size
172 distribution surface plots showing jointly the variation in particle diameter and particle number
173 concentration density in time were also derived. Identification and classification of NPF and
174 growth events was accomplished on these surface plots (Dal Maso et al., 2005; Németh et al.,
175 2018) on a daily basis into the following main classes: NPF event days, non-event days, days
176 with undefined character, and days with missing data (for more than 4 h during the midday).
177 Relative occurrence frequency of events was determined for each month and year as the ratio
178 of the number of event days to the total number of relevant (i.e. all–missing) days. A subset of
179 NPF events with uninterrupted evolution in time, which are called quantifiable (class 1A)
180 events, were further separated because the time evolution of their size distribution functions
181 was utilised to determine the dynamic and timing properties with good accuracy and reliability.

182

183 **3.1 Dynamic and timing properties**

184

185 Growth rate (GR) of nucleation-mode particles was calculated by mode-fitting method
186 (Kulmala et al., 2012). Particle number median mobility diameter (NMMD) of the nucleation
187 mode were obtained from fitting the individual size distributions by DoFit algorithm (Hussein
188 et al., 2004). The growth rate was determined as the slope of the linear line fitted to the time
189 series of the NMMD data within a time interval around a diameter d , where the dependency
190 could be satisfactorily approximated by linear fit. Since the nucleation mode was mostly
191 estimated by N_{6-25} in the calculations of the formation rate (see below), and since the median
192 of the related diameter interval (from 6 to 25 nm) is close to $d=10$ nm, GRs for particles with a
193 diameter of 10 nm were determined (GR_{10}). This type of GR can be interpreted as an average
194 GR as far as the given particle diameter range is concerned, but it actually expresses the
195 beginning of the growth process only. Particle growth can slow substantially in time in specific
196 cases, and this can affect considerably the formation rate calculations (see later).

197

198 Time evolution of an aerosol population is described by the general dynamic equation which
199 was rearranged, simplified and approximated by several quantities (Kulmala et al., 2001; Dal
200 Maso et al., 2002; Kulmala et al., 2012; Cai and Jiang, 2017) to express the formation rate J_6
201 of particles with the smallest detected diameter of $d_{\min}=6$ nm in a form utilised in the present
202 evaluation as

203

$$204 \quad J_6 = \frac{dN_{6-25}}{dt} - \frac{dN_{Ai,<25}}{dt} + \text{CoagS}_{10}(N_{6-25} - N_{Ai,<25}) + \frac{\text{GR}_{10}}{(25-6)}(N_{6-25} - N_{Ai,<25}). \quad (1)$$

205

206 The first term on the right side of Eq. 1 expresses the concentration increment. The particle
207 number concentration in the size range from 6 to 25 nm (i.e. N_{6-25}) is usually selected to
208 approximate the nucleation-mode particles $N_{\text{nuc}} \approx N_{6-25}$. This is a reasonable choice because it
209 was proved to be advantageous and effective way in handling fluctuating data sets since N_{6-25}
210 often exhibits smaller scatter in time and less sensitivity than the fitted area of the nucleation
211 mode. It is implicitly assumed that the intensity of the NPF is constant for a certain time interval,
212 and, therefore, dN_{6-25}/dt can be determined as the slope of the linear function of N_{6-25} versus
213 time t within an interval where the dependence could be satisfactorily approximated by linear
214 fit. A limitation of the relatively wide size range (6–25 nm) selected can be manifested by
215 disturbances from primary particles particularly in urban environments. This is taken into
216 account by an additional term of $N_{Ai,<25}$, which is discussed below.

217

218 The second term on the right side of Eq. 1 expresses the contribution of high-temperature
219 emission sources, usually of vehicular road traffic (Paasonen et al., 2016; Salma et al., 2017) to
220 N_{6-25} , which can provisionally disturb the assumption of $N_{\text{nuc}} \approx N_{6-25}$. A typical example of such
221 a situation is shown in Fig. S1a from 10:09 to 12:23 LT. In these specific cases, the contribution
222 of primary emissions was estimated from the slope of the time series of the fitted peak area of
223 the Aitken mode below $d < 25$ nm ($N_{Ai,<25}$) in the time region under consideration. Reliable
224 separation of the nucleation and Aitken modes from each other was hindered or was not possible
225 for a few individual size distributions due to overlapping modes and the scatter in the measured
226 concentration data, and these individual cases were excluded from or skipped in the time series.

227

228 The third term on the right side of Eq. 1 represents the loss of particles due to coagulation
229 scavenging (with pre-existing particles). The coagulation scavenging efficiency for particles
230 with a diameter of 10 nm (CoagS_{10}) was selected to approximate the mean coagulation
231 efficiency of nucleation-mode particles ($\text{CoagS}_{\text{nuc}}$). This diameter was chosen by considering
232 the median of the related diameter range, which was discussed above for GR. The coagulation
233 efficiency was calculated from classical aerosol mechanics with adopting a mass
234 accommodation coefficient of 1 and utilizing the Fuchs' transition-regime correction factor
235 (Kulmala et al., 2001; Dal Maso et al., 2005; Kulmala et al., 2013) by using computation scripts

236 developed at the University of Helsinki. Self-coagulation within the nucleation mode was
237 neglected due to limited ambient concentrations. Hygroscopic growth of particles was not
238 considered since this depends on chemical composition of particles, which is unknown.

239

240 The fourth term on the right side of Eq. 1 expresses the growth out of newly formed particles
241 from the size range by condensation of vapours. The GR_{10} was selected to approximate a
242 representative value at the median of the particle diameter range considered (Vuollekoski et al.,
243 2012). It is implicitly assumed that GR_{10} can be regarded to be constant over the time interval
244 under consideration. Nevertheless, the growth of nucleation-mode particles in time is
245 occasionally limited (Fig. S1b). In these specific cases, the mean relative area of the nucleation
246 mode below 25 nm was determined by fitting individual size distributions around the time of
247 the maximum nucleation-mode NMMD, and the ratios were averaged. A correction in form of
248 the mean relative area was adopted as a multiplication factor for the growth out term in Eq. 1.
249 On very few days, the growth of newly formed particles was followed by a decrease in
250 nucleation-mode NMMD (Salma et al., 2016a). In these cases, the shrinkage rate (with a formal
251 $GR_{10}<0$) was derived and adopted in Eq. 1. Relative contributions of the concentration
252 increment, coagulation loss and growth out from the diameter interval to J_6 are decreasing in
253 this order with mean values of 71%, 17% and 12%, respectively (Table S1).

254

255 The formation and growth rates for the measurement years of 2008–2009 and 2012–2013 were
256 calculated earlier by a slightly different way and neglecting the urban features discussed above
257 (Salma et al., 2011, 2016b). To obtain consistent data sets, the dynamic properties for these 2
258 years were re-evaluated by adopting the present improved protocol and implementing the
259 experience gained over the years. The mean new-to-old rate ratios with SDs for the GR_{10} and
260 J_6 were 1.06 ± 0.32 and 1.23 ± 0.37 , respectively in the city centre (2008–2009) and 1.04 ± 0.21
261 and 1.20 ± 0.35 , respectively in the near-city background (2012–2013). It was the smaller rates
262 that were primarily and sometimes substantially impacted. The modifications were
263 simultaneously adopted. The subtraction of particle number concentrations emitted by road
264 traffic from N_{6-25} usually leads to a decrease in the coagulation loss term and loss term due to
265 growth out from the diameter range of 6–25 nm. At the same time, the subtraction can also
266 influence the slope of the concentration change in time (dN_{nuc}/dt) depending on the actual time
267 evolution of perturbing emission source. In addition to that, the time interval in which this slope
268 is considered to be constant was set in a new treatment. It is noted that the relative contributions
269 of the concentration increment, coagulation loss and growth out from the diameter interval to

270 J_6 have different weights in propagating their effects. Furthermore, J_6 itself also depends on
271 GR_{10} , which makes the relationships even more complex. These connected effects explain why
272 the changes resulted in increments. The re-calculation is considered as a methodological
273 improvement over the years of research.

274

275 The assumptions and estimations above usually represent a reasonable approximation to reality.
276 The N_{6-25} is derived from the experimental data in a straightforward way, the GR_{10} and the
277 corrections for primary particles and limited particle growth depend on the quality of the size
278 distribution fitting as well, while the $CoagS_{10}$ is determined by using a theoretical model. The
279 resulting accuracies of the dynamic properties, in particular of J_6 , look rather complicated. They
280 also depend on the spatial heterogeneity in the investigated air masses particularly for the
281 observations performed at the fixed site, size and time resolution of the concentrations
282 measured, diameter range of the size distributions, fluctuations in the experimental data,
283 selection of the particle diameter interval, choice of the time interval of interest (for linear fits),
284 sensitivity of the models to the input uncertainties (Vuollekoski et al., 2012), and also on the
285 extent of the validity of the assumptions applied under highly polluted conditions (Cai and
286 Jiang, 2017). The situation is further complicated with the fact that the dynamic (and also the
287 timing) properties are connected to each other. Finally, it is important to recognise that some
288 NPF and growth curves on the surface plots have rather broad starting time interval (Fig. S1b
289 and S1c). They occur in a considerable abundance in cities, e.g. in 40% of all quantifiable events
290 in Budapest (Sect. 4.4). This may yield badly defined or composite dynamic properties, whose
291 uncertainty can have principle limitations which can prevail on the experimental and model
292 uncertainties.

293

294 Timing properties of NPF and growth events are increasingly recognised, and they can provide
295 valuable information even if they are estimated indirectly from the observed diameter interval
296 >1.5 nm (Sect. 1). The earliest estimated time of the beginning of a nucleation (t_1) and the latest
297 estimated time of the beginning of a nucleation (t_2) were derived by a comparative method
298 (Németh and Salma, 2014) based on the variation in the content of the first size channel of the
299 DMPS system. Both time parameters include a time shift that accounts for the particle growth
300 from the stable neutral cluster mode at approximately 2 nm to the smallest detectable diameter
301 limit of the DMPS systems (6 nm in our case) by adopting the GR value in the size window
302 nearest to it in size space. The difference $\Delta t = t_2 - t_1$ is considered as the duration time interval of
303 the nucleation process. It represents the time interval during which new aerosol particles are

304 generated in the air. The timing properties are expressed in UTC+1, and their uncertainty is
305 regarded to be ca. 30 min under ordinary NPF and growth situations.

306

307 **3.2 Sources and sink**

308

309 Relative effects and role of gas-phase H₂SO₄ were estimated by its proximity measure (proxy
310 value) containing both its major source and sink terms under steady-state conditions according
311 to Petäjä et al. (2009). It was calculated for GRad>10 W m⁻². Formally, it is possible to convert
312 the H₂SO₄ proxy values to H₂SO₄ concentrations by an empirical scaling factor of $k=1.4\times 10^{-7}\times\text{GRad}^{-0.70}$,
313 where GRad is expressed in a unit of W m⁻² (Petäjä et al., 2009). The factor was,
314 however, derived for a remote boreal site, and, therefore, we prefer not to perform the
315 conversion since urban areas are expected to differ from the boreal regions. The conversion was
316 applied only to estimate the order of average H₂SO₄ atmospheric concentration levels. The
317 results derived by utilising the proxy are subject to larger uncertainties than for the other
318 properties because of these limitations, but they may indicate well gross tendencies.

319

320 Condensation sink for vapour molecules onto the surface of existing aerosol particles was
321 computed for discrete size distributions as described in earlier papers (Kulmala et al., 2001; Dal
322 Maso et al., 2002, 2005) and summarised by Kulmala et al. (2013). The equilibrium vapour
323 pressure of the condensing species was assumed to be negligible at the surface of the particles,
324 thus similar to sulfuric acid. Dry particle diameters were considered in the calculations.

325

326 **4 Results and discussion**

327

328 Annual median total particle number concentrations (*N*) for each measurement year are
329 summarised in Table 1. The data for the city centre indicate a moderate decreasing trend. The
330 mean UF/*N* ratio with SD for the same measurement time intervals were 67±14%, and 79±6%,
331 75±10%, 75±11%, 76±11% and 80±10%, respectively. The values correspond to ordinary
332 urban atmospheric environments in Europe (Putaud et al., 2010, Sun et al., 2019). An overview
333 on the number of classified days for each measurement year is also given in Table 1. The
334 availability of the daily size distribution surface plots with respect to all days ensures that the
335 data are representative on yearly and monthly time scales, except for the months August and
336 September 2015, when there were missing days in larger ratios. The number of quantifiable

337 event days (248 cases) is also considerable, which establishes to arrive at firm conclusion for
 338 the NPF and growth events as well.

339

340 **Table 1.** Annual median total particle number concentrations (in 10^3 cm^{-3}), number of days with NPF
 341 and growth event, quantifiable event days, non-event days, undefined days, missing days and the
 342 coverage (in %) of relevant days in the near-city background and city centre separately for the 1-year
 343 long measurement time intervals.

344

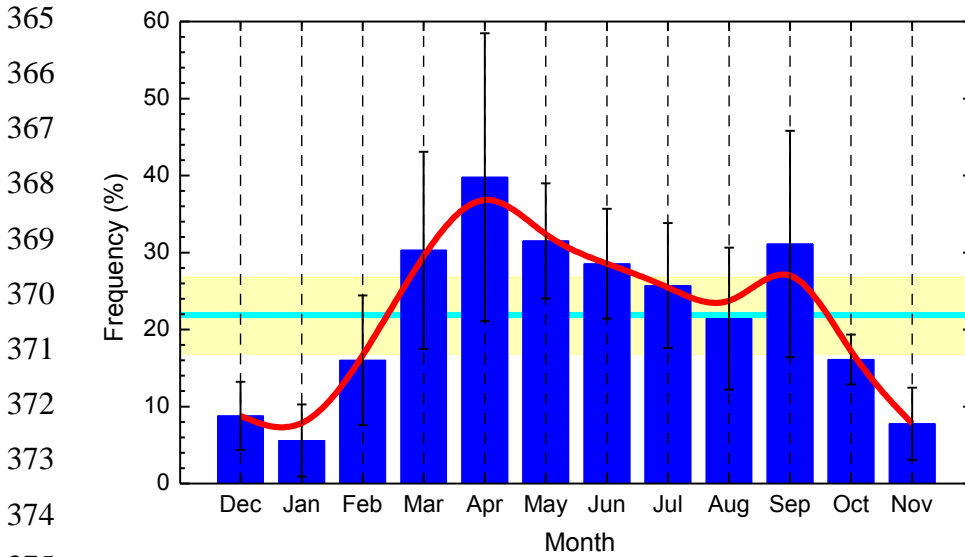
Environment	Background		Centre				
	Time interval	2012–2013	2008–2009	2013–2014	2014–2015	2015–2016	2017–2018
Concentration		3.4	11.5	9.7	9.3	7.5	8.7
Event days		96	83	72	81	35	83
Quantifiable days		43	31	48	56	18	52
Undefined days		19	34	24	25	8	23
Non-event days		231	229	267	240	226	257
Coverage		95	95	99	95	73	99
Missing days		20	19	2	19	97	2

345

346 It was previously shown that the NPF and growth events observed in the city centre of Budapest
 347 and its background ordinarily happen above a larger territory or region in the Carpathian Basin
 348 (Németh and Salma, 2014), and they are linked to each other as a spatially coherent and joint
 349 atmospheric phenomenon (Salma et al., 2016b). From the point of the occurrence frequency
 350 distribution, they can, therefore, be evaluated jointly in the first approximation. An overall
 351 monthly mean relative occurrence frequency of nucleation days derived for all 6 measurement
 352 years is shown in Fig. 1. The annual mean frequency with SD was $22 \pm 5\%$, which is considerable
 353 and is in line with other urban sites (Sect. 1). The monthly mean frequency has a temporal
 354 variation, which can be characterised by a noteworthy pattern. The mean monthly dependency
 355 exhibits an absolute and a local minimum in January (5.6%) and August (21%), respectively,
 356 and an absolute and a local maximum in April (40%), and September (31%), respectively.
 357 Nevertheless, the SDs of the monthly means indicate prominent variability from year to year.
 358 The pattern can be related to multivariate relationships and complex interplay among the
 359 influencing factors, which include the air temperature (January is the coldest month, while
 360 August is the warmest month in the Carpathian Basin) and enhanced emission of biogenic
 361 VOCs in springtime (March–April) and early autumn (September) as well (Salma et al., 2016b).

362 It is noted that the findings derived for the separate city-centre data set are very similar to the
363 results presented above.

364



374

375
376 **Figure 1.** Monthly mean relative occurrence frequency of NPF and growth events for the joint 6-year
377 long data set. The error bars show ± 1 standard deviation, the horizontal line in cyan indicates the overall
378 annual mean frequency, the yellow bands represent ± 1 standard deviation of the annual mean, and the
379 smooth curve in red serves to guide the eye.

380

381 The properties and variables studied were derived in full time resolution. They were averaged
382 in several ways for different conditions and for various purposes to obtain typical average
383 descriptive characteristics. In 1 case (31–08–2016), the NPF and growth event could reliable
384 be identified, while the measured absolute particle number concentrations could not be
385 validated due to experimental troubles, and, therefore, it was left out from the further
386 calculations. Similarly, there were 1 and 4 events with unusually/extraordinarily large dynamic
387 properties in the measurement years 2014–2015 and 2017–2018, respectively. More
388 specifically, 5 individual J_6 data when expressed in a unit of $\text{cm}^{-3} \text{ s}^{-1}$ and 1 individual GR_{10}
389 data when given in nm h^{-1} were >20 (Table 3). These extremes were left out from the overview
390 statistics to maintain the representativity (they could be influenced by some unknown extra or
391 very local sources) and to fulfil better the basic requirements of correlation analysis. If an event
392 showed a double beginning then the dynamic properties for the first onset were considered in
393 the basic overview since this onset is of regional relevance (Salma et al., 2016b). The extreme
394 NPF and growth events and the characteristics for the second onsets were, however, evaluated
395 separately and are discussed in detail and interpreted in Sect. 4.4.

396 **4.1 Ranges and averages**

397

398 Ranges and averages with SDs of formation rate J_6 , growth rate GR_{10} , starting time of
399 nucleation (t_1) and duration time interval of nucleation (Δt) are summarised in Table 2 for
400 separate measurement years and for the joint 5-year long city centre data set. In the city centre,
401 nucleation generally starts at 09:15 UTC+1, and it is typically maintained for approximately 3
402 h. The NPF and growth events ordinarily produce 5.6 new aerosol particles with a diameter of
403 6 nm in 1 cm³ of air in 1 s, and cause the particles with a diameter of 10 nm to grow with a
404 typical rate of 7.6 nm h⁻¹. The statistics for J_6 and GR_{10} are based on 199 and 203 events,
405 respectively. The corresponding data for the separate years show considerable variability
406 without obvious trends or tendencies. The differences between the years can likely be related
407 to changes in actual atmospheric chemical and physical situations and conditions, and to the
408 resulting modifications in the sensitive balance and delicate coupling among them from year to
409 year. Spread of the individual data for GR_{10} is smaller than for J_6 ; the relative SDs for the joint
410 5-year long city centre data set were 38% and 68%, respectively.

411

412 The dynamic properties and t_1 data tend to be smaller in the near-city background than in the
413 city centre. In general, nucleation starts 1 h earlier in the background, and the events typically
414 show significantly smaller J_6 (with a median of 2.0 cm⁻³ s⁻¹) and GR_{10} (with a median of 5.0
415 nm h⁻¹). Duration of the nucleation is very similar to that in the city centre. All starting times
416 of nucleation were larger than (in a few cases, very close to) the time of the sunrise. This implies
417 that no nocturnal NPF and growth event has been identified in Budapest so far. The particle
418 growth process (the so-called banana curve) could be traced usually for a longer time interval
419 (up to 1.5 d) in the background than in the centre.

420

421 These results are in line with the ideas on atmospheric nucleation and consecutive particle
422 growth process (e.g. Kulmala et al., 2014; Zhang et al., 2015; Kerminen et al., 2018). It was
423 observed in a recent overview study (Nieminen et al., 2018) that the formation rate of 10–25
424 nm particles increased with the extent of anthropogenic influence, and in general, it was 1–2
425 orders of magnitude larger in cities than at sites in remote and clean environments.

426

427 **Table 2.** Ranges, averages and standard deviations of aerosol particle formation rate J_6 , particle diameter
 428 growth rate GR_{10} , starting time (t_1) and duration time interval ($\Delta t=t_2-t_1$) of nucleation process of
 429 quantifiable NPF and growth events in the near-city background and city centre separately for the 1-
 430 year long measurement time intervals and for the joint 5-year long city centre data set.
 431

Environment	Background		Centre				
	2012– 2013	2008– 2009	2013– 2014	2014– 2015	2015– 2016	2017– 2018	All 5 years
Formation rate J_6 ($\text{cm}^{-3} \text{s}^{-1}$)							
Minimum	0.48	1.47	1.13	0.81	1.19	1.60	0.81
Median	2.0	4.2	3.5	4.4	4.6	6.3	4.6
Maximum	5.6	15.9	17.8	18.0	15.3	17.3	18.0
Mean	2.2	4.7	5.2	5.6	5.0	6.6	5.6
St. deviation	1.3	2.6	3.7	4.2	3.7	3.3	3.8
Growth rate GR_{10} (nm h^{-1})							
Minimum	3.0	3.7	3.1	2.8	3.2	3.3	2.8
Median	5.0	7.6	6.6	6.5	8.0	7.5	7.3
Maximum	9.8	17.4	19.0	18.0	15.5	19.8	19.8
Mean	5.2	7.8	7.2	7.3	7.7	8.0	7.6
St. deviation	1.4	2.6	2.8	3.2	3.0	2.8	2.9
Starting time, t_1 (HH:mm UTC+1)							
Minimum	05:51	07:14	06:44	05:48	07:31	05:57	05:48
Median	08:19	09:26	09:22	08:48	09:45	09:18	09:15
Maximum	11:09	11:38	12:21	11:23	12:45	12:15	12:45
Mean	08:17	09:27	09:25	08:49	10:02	09:24	09:19
St. deviation	01:11	01:05	01:26	01:22	01:23	01:36	01:26
Duration time, Δt (HH:mm)							
Minimum	01:23	00:52	00:42	00:31	01:03	01:26	00:31
Median	03:16	02:36	02:04	03:53	02:31	03:49	02:57
Maximum	06:44	06:04	05:34	07:46	06:05	07:55	07:55
Mean	03:30	02:44	02:14	03:52	02:58	03:57	03:18
St. deviation	01:40	01:11	01:01	01:40	01:47	01:39	01:40

432
 433 Ranges and averages with SDs of some related atmospheric properties, namely of mean CS
 434 averaged for the time interval from t_1 to t_2 , daily maximum gas-phase H_2SO_4 proxy, daily mean
 435 T and RH (Table S2), and of daily median concentrations of SO_2 (as the major precursor of gas-
 436 phase H_2SO_4), O_3 (as an indicator of photochemical activity), NO_x and CO gases (as indicators
 437 of anthropogenic combustion activities and road vehicle emissions) (Table S3) were also
 438 derived for quantifiable NPF and growth event days, and are further evaluated. The annual
 439 mean CS values exhibited decreasing tendency in the city centre over the years. The individual

440 values remained below approximately $20 \times 10^{-3} \text{ s}^{-1}$, which agrees well with the results of our
441 earlier study (Salma et al., 2016b) according to which the CS suppresses NPF above this level
442 in the Carpathian Basin. Maximum H_2SO_4 proxy values reached substantially higher levels (by
443 a factor of approximately 2) in the near-city background than in the city centre due mainly to
444 the differences in the CS and $[\text{SO}_2]$. The differences between the 2 sites are particularly evident
445 when considering their smallest values. The largest variability in the annual average values
446 were observed for the proxy. Median concentration of H_2SO_4 molecules was roughly estimated
447 to be approximately $5 \times 10^5 \text{ cm}^{-3}$ by adopting the scaling factor (Sect. 3.2). The air T displayed
448 quite similar and comparable values over the years at both sites. The discussion of its overall
449 effect on the dynamic properties is accomplished in Sec. 4.2, where the monthly distributions
450 are presented. Some events happened at daily mean temperatures below zero. The daily mean
451 RH and its SD for the city centre and near-city background were $54 \pm 11\%$ and $64 \pm 12\%$,
452 respectively. There were events that occurred at RHs as high as 90%. Relationships of the
453 dynamic properties with T and RH are also obscured with strong seasonal cycle of these
454 meteorological data and with the fact that air masses arriving to the receptor site in different
455 trajectories are often characterised by distinct levels of meteorological data.

456
457 As far as the pollutant gases are concerned (Table S3), SO_2 showed somewhat smaller daily
458 median values, and O_3 exhibited substantially smaller levels on event days in the city centre
459 than in the near-city background, while concentrations of NO_x and CO were obviously larger
460 in the city than in its close background. The differences can primarily be explained by intensity
461 and spatial distribution of their major sources and atmospheric chemical reactions, and the
462 joined concentration data resembles typical situations without photochemical smog episodes in
463 cities. There was no obvious decrease in SO_2 concentration during these years in contrast with
464 an earlier decreasing trend from mid-1980s till about 2000.

465

466 **4.2 Monthly distributions**

467

468 Distributions of the monthly mean J_6 , GR₁₀, daily maximum gas-phase H₂SO₄ proxy, mean CS,
469 daily mean air T and RH, and daily median SO₂, O₃, NO_x and CO concentrations for quantifiable
470 NPF and growth events for the joint city centre data sets are shown in Fig. 2. The distributions
471 – eminently for J_6 , GR₁₀, H₂SO₄ proxy and SO₂ – do not follow the monthly pattern of the event
472 occurrence frequency at all (cf. Fig. 1). Instead, the J_6 , GR₁₀ and H₂SO₄ proxy tend to exhibit
473 larger values in summer months, and they temporal changes over the other months are smooth
474 and do not show distinctive features. The elevations are substantial; the estimated maximum
475 level was larger than the baseline by a factor of 2.1 for the J_6 , and by a factor of approximately
476 1.4 for the GR₁₀ and H₂SO₄ proxy. Intensity of solar radiation, its seasonal cycling,
477 concentration of atmospheric precursors in different months, biogenic processes, anthropogenic
478 activities and the fact that rate coefficients of many thermal chemical/physicochemical
479 processes in the nature (including GR, Paasonen et al., 2018) increase with T could play an
480 important role in explained the distributions.

481

482 The differences in the GRad (and some other properties) are, however, biased by the seasonal
483 cycle of solar electromagnetic radiation via the seasonal variation of NPF occurrence frequency.
484 Nevertheless, the misalignment among the monthly distributions of NPF and growth event
485 occurrence frequency and all the other properties indicates that the occurrence or its basic
486 causes are not linked with the dynamic properties in a straightforward or linear manner in the
487 Carpathian Basin including Budapest.

488

489 Some of our results are in line with other observations according to which GR exhibited almost
490 exclusively a summer maximum, while some other finding are different in the sense that the
491 seasonal variability in particle formation rate was quite modest and could not be established
492 earlier (Nieminen et al., 2018). There is one more aspect which may be worth realising in this
493 respect. A large fraction of compounds contributing to NPF and growth in cities can originate
494 from anthropogenic precursors (Vakkari et al., 2015). Their emissions may peak any time of
495 year depending on human habits and requirements (Nieminen et al., 2018). Nevertheless, the
496 fact that our monthly distributions of the dynamic properties in urban environments follow the
497 universal summer maximum behaviour may indicate the overall prevailing role of atmospheric
498 photochemistry coupled with biogenic emissions of aerosol precursor vapours.

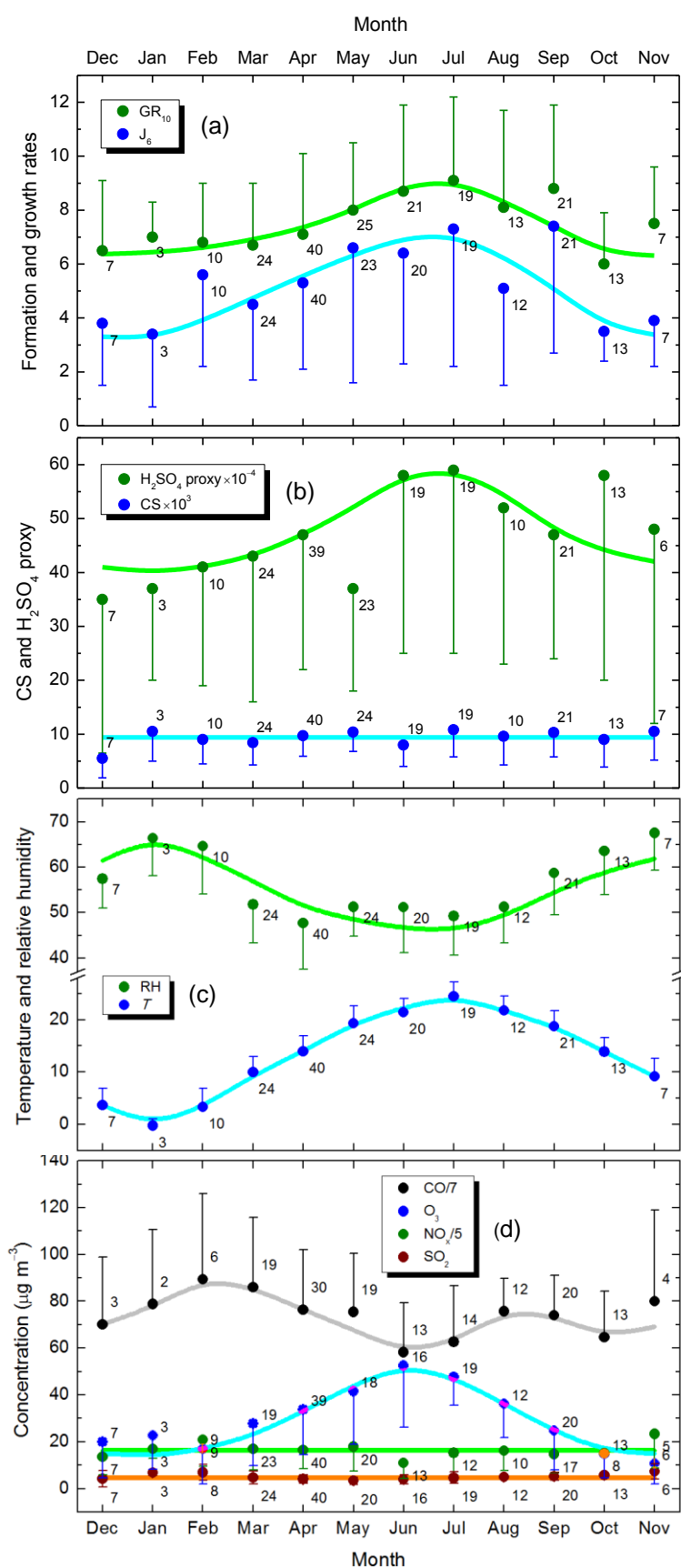
499

500 The monthly mean J_6 , GR_{10} and H_2SO_4 proxy data still have considerable uncertainty, which
501 makes their interpretation not yet completely conclusive. The uncertainties are influenced by
502 inherent fluctuations in the primary data sets, enhancing effects caused by combining some
503 individual primary data into compound variables (such as H_2SO_4 proxy), number of data items
504 available for different properties and months, variations in other or unknown relevant
505 environmental conditions, and by the variability in relative nucleation occurrence frequency
506 from year to year. The resulting uncertainties are expected to decrease with the length of the
507 available data sets, which emphasized the need to continue the measurements.

508

509 The monthly distributions of CS, and SO_2 and NO_x concentrations could be represented by
510 constant values of the overall means and SDs of $(9.4 \pm 4.3) \times 10^{-3} s^{-1}$, $4.7 \pm 2.1 \mu g m^{-3}$ and 81 ± 38
511 $\mu g m^{-3}$, respectively with an acceptable accuracy. This suggests that these variables in Budapest
512 do not critically or substantially affect the dynamic properties (or the event occurrence).
513 Monthly distributions of air T and O_3 concentration showed a maximum over summer months,
514 while RH reflected the T tendency. In addition, monthly averages of T on event days and on
515 non-event days were similar. Both higher biogenic emissions and typically stronger
516 photochemistry are expected during the summer, which enhance the production rate of
517 nucleating and condensing vapours, while there is practically nothing extra in the first
518 approximation (except for extreme T s) that would suppress the dynamical properties (Kerminen
519 et al., 2018). As result of these complex effects, the dynamic rates showed a summer maximum.
520 This is consistent with the results from other urban and non-urban studies (Nieminen et al.,
521 2018). Distribution of CO was more changing and without obvious tendentious temporal
522 structure or feature than for the other gases, and, therefore, its interpretation is encumbered so
523 far. However, it doesn't seem to substantially affect the dynamic properties.

524



526 **Figure 2.** Distribution of
 527 monthly mean aerosol
 528 particle formation rate J_6 in
 529 a unit of $\text{cm}^{-3} \text{s}^{-1}$ and
 530 particle diameter growth
 531 rate GR_{10} in a unit of nm h^{-1}
 532 (a), mean condensation sink
 533 for vapours (CS) in a unit of
 534 s^{-1} averaged over the
 535 nucleation time interval (t_1 ,
 536 t_2) and daily maximum gas-
 537 phase H_2SO_4 proxy in a unit
 538 of $\mu\text{g m}^{-5} \text{W s}$ (b), daily
 539 mean air temperature (T) in
 540 a unit of $^\circ\text{C}$ and daily mean
 541 relative humidity (RH) in %
 542 (c), and daily median
 543 concentrations of SO_2 , O_3 ,
 544 NO_x and CO for
 545 quantifiable NPF and
 546 growth events in the city
 547 centre for the joint 5-year
 548 long time interval. The error
 549 bars are shown for one side
 550 and indicate 1 standard
 551 deviation. Number of the
 552 individual data averaged in
 553 each month is displayed
 554 next to the symbols. The
 555 horizontal lines indicate the
 556 overall mean. The nonlinear
 557 curves assist to guide the
 558 eye.

560 Distributions of monthly mean ratios of major variables on NPF event days to that on non-event
561 days for the joint city centre data set are summarised in Fig. 3. It is noted that the differences in
562 the number of non-event days and event days are the largest in winter and smallest in spring
563 (Fig. 1). The annual mean ratios for N_{6-100} , GRad, SO_2 and O_3 were above unity, for $N_{100-1000}$
564 and RH, they were below unity, while the value of CS, NO_x and CO were close to each other
565 on both types of days. Ultrafine particles are generated by NPF and growth processes in a
566 considerable amount; their concentration was larger by 23% on event days than on non-event
567 days. This agrees with our earlier assessment of the NPF contribution as a single source of
568 particles based on nucleation strength factor NSF_{GEN} of 13% as a lower estimate (Salma et al.,
569 2017). The other variables of the first group above represent conditions which favour
570 atmospheric nucleation and particle growth, i.e., strong solar radiation, precursor gas and
571 general photochemical activity, respectively. Particles in the size range of 100–1000 nm (the
572 pre-existing particles with a relatively long residence time) express a condensation and
573 scavenging sink, which represents a competing process to nucleation. There is also evidence
574 that RH acts against continental NPF process (Hamed et al., 2011).

575

576 It is also seen in Fig. 3 that NPF and growth events in winter took place preferably when N_{100-}
577 $_{1000}$, CS, RH, NO_x , and CO concentrations were especially low and O_3 concentration was
578 unusually large. It can be explained by considering that the basic preconditions of NPF events
579 are realised by the ratio of source and sink terms for condensing vapours. The source strength
580 in winter is often decreased substantially in the Budapest area (Salma et al., 2017) due to lower
581 solar radiation and less (biogenic) chemical precursors in the air. Nevertheless, NPF can still
582 occur if the sink becomes even smaller. This also explains the lower event day-to-non-event
583 day ratios for N_{6-100} observed in winter months. Full exploitation of the data base by
584 multistatistical and other methods has been in progress and is to be published in a separate
585 article.

586

587
 588
 589
 590
 591
 592
 593
 594
 595
 596
 597
 598
 599
 600
 601
 602
 603
 604
 605
 606
 607
 608
 609
 610
 611
 612
 613
 614
 615
 616
 617
 618
 619
 620

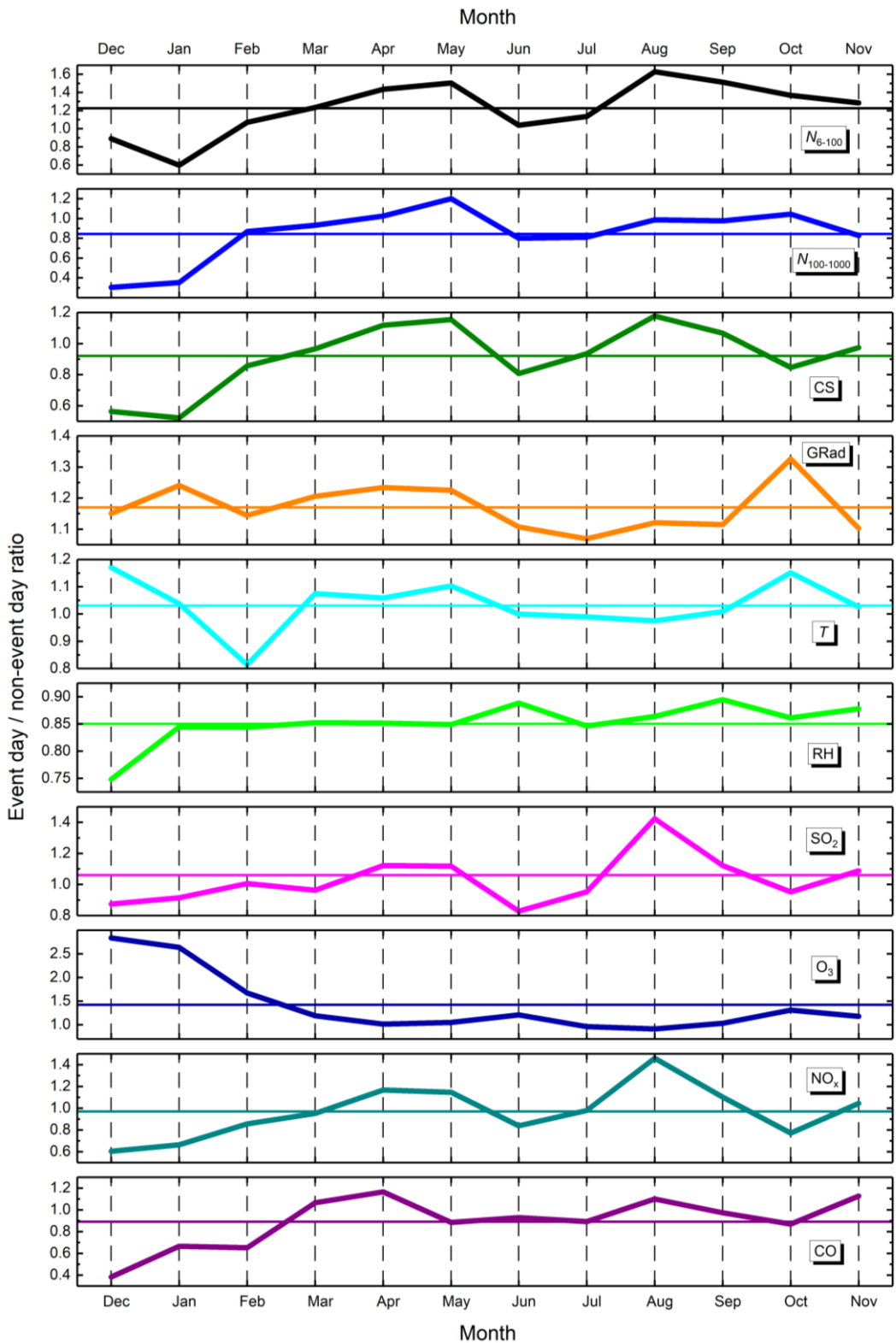


Figure 3. Distributions of monthly mean ratios of median concentrations of N_{6-100} , $N_{100-1000}$, SO_2 , O_3 , NO_x and CO, and of mean condensation sink for vapours (CS), global solar radiation (GRad), air temperature (T) and relative humidity (RH) on NPF event days to that on non-event days in the city centre for the joint 5-year long time interval. The horizontal lines represent annual average ratios.

621 4.3 Relationships

622

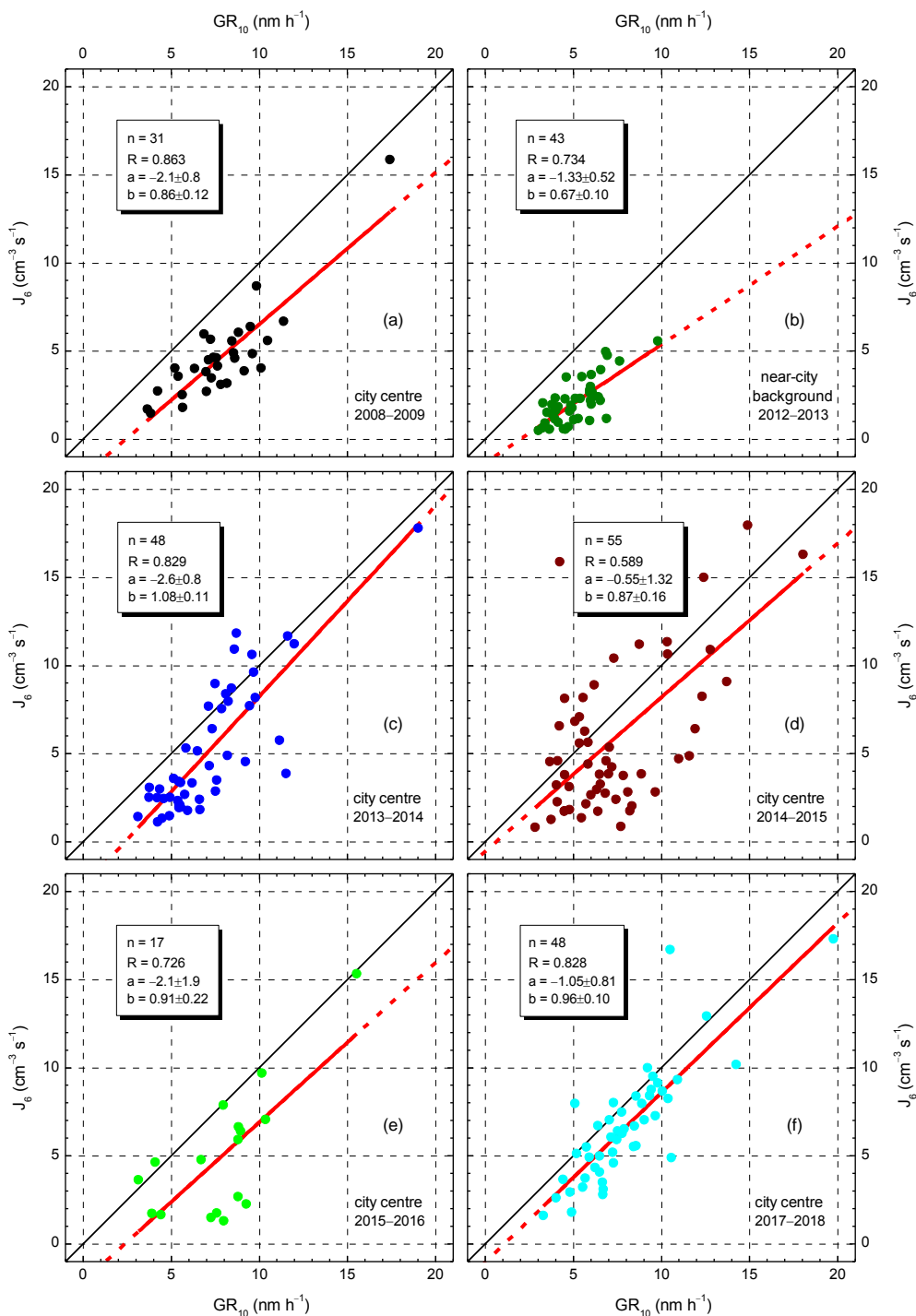
623 Pearson's coefficients of correlation (R) between J_6 and GR_{10} revealed significant linear
624 relationship between them for all annual data sets (the mean R and SD were 0.768 ± 0.099 ,
625 number of data pairs $n=243$). This confirms that formation of new aerosol particle and their
626 growth to larger sizes are tightly and positively linked together. It should be noted that J_6 and
627 GR_{10} are not completely independent variables (see Eq. 1 and Table S1). The linear relationship
628 between the dynamic properties was observed under different atmospheric conditions in many
629 environments (Nieminen et al., 2018).

630

631 The dynamic properties can also be coupled to the concentrations of aerosol precursor
632 compounds and properties of a pre-existing particle population, thus to atmospheric
633 environment (Kerminen et al., 2018). It is, therefore, sensible to investigate the city centre and
634 near-city background data separately. Scatter plots between J_6 and GR_{10} for the 1-year long
635 measurement time intervals are shown in Fig. 4. For the city centre, the regression lines follow
636 the line with a slope of 1 in all 5 years. The mean slope (b) with SD for the joint 5-year long
637 city centre data set was $b=0.94 \pm 0.07$ expressed formally in a unit of $\text{cm}^{-3} \text{s}^{-1} \text{nm}^{-1} \text{h}$. At the
638 same time, the regression line for the near-city background deviated significantly with a
639 $b=0.67 \pm 0.10 \text{ cm}^{-3} \text{s}^{-1} \text{nm}^{-1} \text{h}$ from the J_6 vs. GR_{10} dependency for the city centre. This can
640 imply that NPF and growth processes advance in a different manner in these 2 environments.
641 This is likely related to the differences between the city and its close environment as far as the
642 atmospheric composition (for instance, the VOC and NO_x concentrations), chemistry and
643 physics, and other delicate conditions are concerned (Paasonen et al., 2018). The narrower
644 range and smaller number of individual dynamic properties available for the near-city
645 background relative to those in the city centre represent some inherent limitation or weakness
646 in the explanation, and, therefore, it can strictly be regarded as a working hypothesis.

647

648
 649
 650
 651
 652
 653
 654
 655
 656
 657
 658
 659
 660
 661
 662
 663
 664
 665
 666
 667
 668
 669
 670
 671
 672
 673
 674



675 **Figure 4.** Scatter plots for aerosol particle formation rate J_6 and particle diameter growth rate GR_{10} in
 676 city centre (a and c–f) and near-city background (b) separately for the 1-year long measurement time
 677 intervals. Number of data point (n), their coefficient of correlation (R) and the intercept (a) and slope
 678 (b) of the regression line with standard deviations are also indicated. The lines in black represent the
 679 line with a slope of 1, the solid lines in red show the regression lines, while the dashed parts in red are
 680 extrapolated from the regression line.

681
682 The intercepts (a) of the regression lines were identical for all data sets within their uncertainty
683 interval. The mean intercept and SD were estimated to be $-1.7 \pm 0.8 \text{ cm}^{-3} \text{ s}^{-1}$. This finding is
684 interpreted as the existence of a minimum GR or more exactly of a minimally required GR that
685 leads to $J_6 > 0$. Particles that exhibit at least this level of GR can escape coagulation mainly with
686 larger particles and reach the detectable diameter (6 nm in our case) by condensational growth.
687 The minimal GR was derived as $\text{GR}_{\min} = -a/b$, and its mean and SD are $1.8 \pm 1.0 \text{ nm h}^{-1}$ for the
688 conditions ordinarily present in the Budapest air. Nucleation processes which are initiated under
689 circumstances that cause the newly formed particle with a diameter of 10 nm to grow with a
690 rate $< \text{GR}_{\min}$ are normally not observed. Anyway, these are expected to be events with relatively
691 small J_6 (weak phenomena) due to the relationship between GR_{10} and J_6 . The events with GR
692 larger but close to this limit could be still masked by fluctuating experimental data. Their
693 identification and evaluation can be made feasible by decreasing the lower measurement
694 diameter limit of DMPS systems down to 3 nm, or by different instruments such as particle size
695 magnifier or neutral cluster and air ions spectrometer.

696
697 Correlations between individual H_2SO_4 proxy values on one side and J_6 or GR_{10} on the other
698 side were not significant. This is consistent with the corresponding conclusion of Sect. 4.2 and
699 with the earlier results according to which the mean contribution of H_2SO_4 condensation to the
700 particle GR_{10} was only 12.3% in Budapest (Salma et al., 2016b). The lack of correlation and
701 the average concentrations of SO_2 derived separately for event and non- event days suggest that
702 this precursor gas is ordinarily available in excess and, therefore, it is usually not the lack of
703 SO_2 gas itself, which limits the NPF and growth events in Budapest. Instead, the reaction rate
704 of oxidation of SO_2 to H_2SO_4 in the gas phase - likely governed by photochemical conditions -
705 , and other chemical species than H_2SO_4 can have larger influence on the particle growth. The
706 role of H_2SO_4 in the nucleation process and early particle growth is still determinant or relevant.

707
708 Coefficients of correlation between CS on one side and J_6 or GR_{10} on the other side for the joint
709 city centre data sets were modest ($R=0.41$ and 0.32 , respectively with $n=194$ and 197 ,
710 respectively). This is simply related to the fact that larger GR values are typical for polluted
711 urban air (Kulmala et al., 2017) since particles capable of escaping coagulation scavenging need
712 to grow faster in comparison to cleaner environments, and the enhanced requirements for the
713 growth are linked to increased formation rates as well. It should be noted here that the GR of
714 newly formed particles to larger sizes is primarily coupled to 1) CS, which is further linked to

715 the entire aerosol particle population (including the newly formed particles, thus the NPF itself),
716 2) to the total concentration and some physicochemical properties of non-volatile gaseous
717 compounds and 3) to their production rate in the gas phase from aerosol precursor compounds
718 (e.g. Kerminen et al., 2018). These couplings could result in rather complex behaviour, and
719 their understanding is essential when analysing atmospheric observations.

720
721 As far as the pollutant gases are concerned, no correlation could be identified between J_6 or
722 GR_{10} on one side and the gas concentrations on the other side. The coefficients of correlation
723 between CS and NO_x or CO were modest ($R=0.37$ and 0.42 , respectively with $n=164$ and 152 ,
724 respectively), while correlation of NO_x and CO on one side with WS was also modest but
725 negative ($R=-0.32$ and -0.42 , respectively with $n=167$ and 155 , respectively). The former
726 relationships can be explained by the fact that vehicular road traffic in cities is a considerable
727 and common source of NO_x , CO and primary particles (Paasonen et al., 2016), and the emitted
728 particles largely contribute to CS levels. The latter relationships are linked to the effect of large-
729 scale air mass transport (often connected to high WSs) on urban air pollution or air quality.

730

731 **4.4 Extreme and multiple events**

732

733 The data sets of J_6 , GR_{10} and Δt containing all, 247 individual values each could be
734 characterised by lognormal distribution function. This is demonstrated by log-probability graph
735 for J_6 in Fig. S2 as example. The coefficient of determination, median and geometric standard
736 deviation for J_6 , GR_{10} and Δt data sets were 0.990 , 4.0 cm^{-3} and 2.3 ; 0.993 , 6.8 nm h^{-1} and 1.46 ;
737 and 0.998 , $02:57$ (0.123 d) and 1.74 , respectively. It is noted that the findings derived for the
738 separate city centre data set are very similar to the results presented above.

739

740 One of the major properties of this distribution type is that it contains relatively large individual
741 data with considerably high abundances. There were 5 individual J_6 and 5 individual GR_{10} data
742 above the 98% percentile of the data sets, which belonged to 9 separate NPF and growth events
743 (days). Their specifications, properties and parameters are summarised in Table 3. All these
744 events occurred in the city centre from April to September. The medians of J_6 , GR_{10} , CS and
745 air T for the subsets of these 9 extreme event days were larger by factors of 5.2 , 2.4 , 1.5 and
746 1.4 , respectively than for the city centre data. At the same time, the medians of the other
747 atmospheric properties and concentrations in these 2 respective data sets agreed within
748 approximately 10%. There was a single event associated with an extreme H_2SO_4 proxy (of

749 $23 \times 10^5 \mu\text{g m}^{-5} \text{ W s}$) and relatively low NO_x concentration ($44 \mu\text{g m}^{-3}$), which indicate
750 exceptionally favourable conditions for NPF and growth. In addition to this case, there were
751 only a few days that were characterised by an unusually large CS ($23 \times 10^{-3} \text{ s}^{-1}$) – which could
752 in turn be linked to higher dynamic rates (Sect. 4.3) – or by somewhat larger SO_2 ($8.1 \mu\text{g m}^{-3}$)
753 or lower NO_x concentration ($34 \mu\text{g m}^{-3}$). For all the other events, however, no simple or
754 compound property of the investigated variables could explain the extreme rates. Instead, they
755 may be related to some other chemical species and/or atmospheric processes, which were not
756 including in the present study.

757

758 **Table 3.** Date (in a format of dd–MM–yyyy), new particle formation rate J_6 (in a unit of $\text{cm}^{-3} \text{ s}^{-1}$),
759 particle diameter growth rate GR_{10} (nm h^{-1}), starting time t_1 of nucleation (HH:mm UTC+1), duration
760 time interval $\Delta t = t_2 - t_1$ of nucleation (HH:mm), mean condensation sink CS during the nucleation process
761 (10^{-3} s^{-1}), daily maximum gas-phase H_2SO_4 proxy ($10^4 \mu\text{g m}^{-5} \text{ W s}$), daily mean air temperature T ($^\circ\text{C}$),
762 daily mean relative humidity RH (%), daily median concentrations of SO_2 , O_3 , NO_x ($\mu\text{g m}^{-3}$) and CO
763 (mg m^{-3}) gases, and the type of the onset for extreme quantifiable NPF and growth events. The cells in
764 yellow indicate the values which are above the 98% percentile of the corresponding data sets. N.a.: not
765 available.

766

Date/ property	15– 09– 2009	20– 04– 2014	19– 05– 2015	04– 07– 2015	28– 05– 2017	25– 06– 2017	02– 08– 2017	31– 08– 2017	09– 09– 2017
J_6	15.9	17.8	24	16.3	27	33	30	47	17.3
GR_{10}	17.4	19.0	12.2	18.0	9.2	17.0	11.8	21	19.8
t_1	10:20	08:52	08:52	09:38	06:34	10:18	07:39	10:06	11:38
Δt	01:23	01:42	03:57	02:06	07:15	02:46	06:58	06:19	02:06
Proxy	38	42	25	16	229	41	69	92	45
CS	13.4	8.9	13.7	11.9	6.9	10.5	23	18.2	15.5
T	20	13.0	22	26	20	24	29	23	19.1
RH	60	62	48	40	40	68	49	47	58
SO_2	6.1	2.5	4.4	2.3	3.4	3.1	5.6	8.1	6.6
O_3	16.3	43	n.a.	33	61	56	34	24	12.9
NO_x	69	34	174	70	44	66	n.a.	109	112
CO	0.42	n.a.	0.71	0.33	0.31	0.50	0.97	0.62	0.71
Onset	ordinary	double	broad	ordinary	broad	broad	broad	broad	ordinary

767

768 Each quantifiable NPF and growth event was labelled as ordinary or broad by visual inspection
769 of its beginning part. If the width of the beginning was smaller than approximately 2 h or there
770 was a determinant single growth curve (rib) on the size distribution surface plot then the onset

771 was labelled as ordinary, otherwise as broad (Fig. S1b and S1c for broad onsets). Broad onsets
772 can be generated by 1) long-lasting nucleation process, 2) disrupted and started over nucleation
773 due to changing atmospheric and meteorological conditions or 3) multiple nucleation processes
774 close to each other in time (Salma et al., 2016b). The broad onsets were specified as doublets
775 if the nucleation mode could be separated into 2 submodes by size distribution fitting.
776 Approximately 40% of all quantifiable events had a broad onset. This indicates that events with
777 broad/multiple onsets are abundant in the urban environment, which could be an important
778 difference from remote or clean atmospheres.

779

780 For ca. 10% of all quantifiable event days, it was feasible to calculate 2 sets of dynamic
781 properties for onsets 1 and 2 with a reasonable accuracy. In the near-city background, the
782 medians of J_6 and GR_{10} for the onset 1 were similar to the corresponding medians for the whole
783 near-city background data set, while for the onset 2, they were substantially larger, namely 4.1
784 $\text{cm}^{-3} \text{s}^{-1}$ and 10.0 nm h^{-1} , respectively (cf. Table 2). Actually, the latter values were closer to
785 the medians of the city centre than for the near-city background. Approximately 75% of the
786 doublets resulted in individual onset2/onset1 ratios larger than unity. Their overall median
787 ratios for J_6 and GR_{10} were similar and approximately 1.2, while for the near-city background,
788 they were about 2. The results are in line with our earlier conclusion according to which the
789 second onsets (if it is a new formation process and not just a started over event) are more
790 intensive than the first onsets (Salma et al., 2016b). These particles also grow faster. This can
791 be explained by the fact that the first event is of regional scale since its dynamic properties
792 resemble those of the regional background (Yli-Juuti et al., 2009), while the later event can be
793 characterised by values typical for the city centre (Salma et al., 2016b). The later event (or
794 events) are mainly caused and governed by sub-regional processes. These findings are also
795 coherent with a previous observation of NPF and growth events with multiple onsets in semi-
796 clean savannah and industrial environments (Hirsikko et al., 2013), and they also fit well into
797 the existing ideas on mixing regional and urban air parcels that exhibit different properties such
798 as precursor concentrations, T and RH (Kulmala et al., 2017).

799

800 **5 Conclusions**

801

802 Magnitude of the particle number concentration level produced solely by NPF and growth can
803 roughly be estimated by considering the median J_6 , median duration of nucleation Δt (their
804 distribution function is lognormal; Table 2) and the mean coagulation loss of these particles

805 F_{coag} (0.17; Sect. 3.1 and Table S1) as: $J_6 \times \Delta t \times (1 - F_{\text{coag}})$. In central Budapest, it yields a
806 concentration of 10^4 cm^{-3} . This is in line with another result achieved by nucleation strength
807 factor (Salma et al., 2017). More importantly, the estimated concentration is comparable to the
808 annual median atmospheric concentrations (Table 1). This simple example indicates that the
809 phenomenon is relevant not only for aerosol load and climate issues on regional or global spatial
810 scales, which were first recognised. It is sensible also to study the effects of NPF and growth
811 events on urban climate and health risk for inhabitants since they produce a large fraction of
812 particles even in cities.

813

814 Similar recognitions have led to emerge of urban atmospheric nucleation studies. As part of this
815 international progress, we presented here a considerable variety of contributions, which became
816 feasible thank to gradually generating, multi-year long, critically evaluated, complex and
817 coherent data sets. Dynamic and timing properties of 247 NPF and growth events were studied
818 together with supporting aerosol properties, meteorological data and pollutant gas
819 concentrations in near-city background and city centre of Budapest for 6 years. The results and
820 conclusions derived form in important component that is based on atmospheric observations.
821 The present study can also be considered as the first step toward a larger and more
822 comprehensive statistical evaluation process.

823

824 Further dedicated research including sophisticated measurements, data evaluations and
825 modelling studies is required to find and identify additional chemical species and their
826 processes, and to account their multifactorial role in more detail. Such measurement campaign
827 focusing on chemical composition of molecular clusters, precursors and nucleating vapours by
828 applying recent expedient instruments in Budapest over the months of the highest expected
829 event occurrence has been just realised within a frame of an international cooperation. Its
830 perspective results can hopefully provide additional valuable information for some of the
831 conclusion base on indirect evidence for the time being and can further clarify the overall
832 picture on urban multicomponent nucleation and growth phenomenon.

833

834 *Data availability.* The observational data used in this paper are available on request from the
835 corresponding author or at the website of the Budapest platform for Aerosol Research and Training
836 (<http://salma.web.elte.hu/BpART>).

837

838 *Author contributions.* I.S. designed the study, performed most of the data analysis, interpreted the
839 results and wrote the paper. Z.N. performed most measurements and data treatment, and contributed to
840 the data analysis.

841

842 *Competing interest.* The authors declare that they have no conflict of interest.

843

844 *Acknowledgements.* The authors thank Markku Kulmala and his research team at the University of
845 Helsinki for their cooperation. Financial support by the National Research, Development and Innovation
846 Office, Hungary (contracts K116788 and PD124283); by the European Regional Development Fund
847 and the Hungarian Government (GINOP-2.3.2-15-2016-00028) is gratefully acknowledged.

848

849 **References**

850 Alam, A., Shi, J. P., and Harrison, R. M.: Observations of new particle formation in urban air, *J.*
851 *Geophys. Res.*, 108 (D3), 4093, doi:10.1029/2001JD001417, 2003.

852 Almeida, J., Schobesberger, S., Kurten, A., Ortega, I. K., Kupiainen-Maatta, O., Praplan, A. P.,
853 Adamov, A., Amorim, A., Bianchi, F., Breitenlechner, M., David, A., Dommen, J., Donahue, N.
854 M., Downard, A., Dunne, E., Duplissy, J., Ehrhart, S., Flagan, R. C., Franchin, A., Guida, R.,
855 Hakala, J., Hansel, A., Heinritzi, M., Henschel, H., Jokinen, T., Junninen, H., Kajos, M.,
856 Kangasluoma, J., Keskinen, H., Kupc, A., Kurten, T., Kvashin, A. N., Laaksonen, A., Lehtipalo,
857 K., Leiminger, M., Leppa, J., Loukonen, V., Makhmutov, V., Mathot, S., McGrath, M. J.,
858 Nieminen, T., Olenius, T., Onnela, A., Petäjä, T., Riccobono, F., Riipinen, I., Rissanen, M., Rondo,
859 L., Ruuskanen, T., Santos, F. D., Sarnela, N., Schallhart, S., Schnitzhofer, R., Seinfeld, J. H.,
860 Simon, M., Sipilä, M., Stozhkov, Y., Stratmann, F., Tome, A., Tröstl, J., Tsagkogeorgas, G.,
861 Vaattovaara, P., Viisanen, Y., Virtanen, A., Vrtala, A., Wagner, P. E., Weingartner, E., Wex, H.,
862 Williamson, C., Wimmer, D., Ye, P. L., Yli-Juuti, T., Carslaw, K. S., Kulmala, M., Curtius, J.,
863 Baltensperger, U., Worsnop, D. R., Vehkamäki, H., and Kirkby, J.: Molecular understanding of
864 sulphuric acid–amine particle nucleation in the atmosphere, *Nature*, 502, 359–363, 2013.

865 Baltensperger, U., Streit, N., Weingartner, E., Nyeki, S., Prévôt, A. S. H., Van Dingenen, R., Virkkula,
866 A., Putaud, J. P., Even, A., Brink, H., Blatter, A., Neftel, A., and Gaggeler, H. W.: Urban and rural
867 aerosol characterization of summer smog events during the PIPAPO field campaign in Milan, Italy,
868 *J. Geophys. Res.*, 107(D22), 8193, doi:10.1029/2001JD001292, 2002.

869 Bianchi, F., Tröstl, J., Junninen, H., Frege, C., Henne, S., Hoyle, C. R., Molteni, U., Herrmann, E.,
870 Adamov, A., Bukowiecki, N., Chen, X., Duplissy, J., Gysel, M., Hutterli, M., Kangasluoma, J.,
871 Kontkanen, J., Kürten, A., Manninen, H. E., Münch, S., Peräkylä, O., Petäjä, T., Rondo, L.,
872 Williamson, C., Weingartner, E., Curtius, J., Worsnop, D. R., Kulmala, M., Dommen, J., and
873 Baltensperger, U.: New particle formation in the free troposphere: A question of chemistry and
874 timing, *Science*, 352, 1109–1112, <https://doi.org/10.1126/science.aad5456>, 2016.

875 Braakhuis, H. M., Park, M. V., Gosens, I., De Jong, W. H., and Cassee, F. R.: Physicochemical
876 characteristics of nanomaterials that affect pulmonary inflammation, *Part. Fibre Toxicol.*, 11:18,
877 doi: 10.1186/1743-8977-11-18, 2014.

878 Cai, R. and Jiang, J.: A new balance formula to estimate new particle formation rate: reevaluating the
879 effect of coagulation scavenging, *Atmos. Chem. Phys.*, 17, 12659–12675, 2017.

880 Carslaw, K. S., Lee, L. A., Reddington, C. L., Pringle, K. J., Rap, A., Forster, P. M., Mann, G. W.,
881 Spracklen, D. V., Woodhouse, M. T., Regayre, L. A., and Pierce, J. R.: Large contribution of
882 natural aerosols to uncertainty in indirect forcing, *Nature*, 503, 67–71, 2013.

883 Crouse, J. D., Nielsen, L. B., Jørgensen, S., Kjaergaard, H. G., and Wennberg, P. O.: Autoxidation of
884 organic compounds in the atmosphere, *J. Phys. Chem. Lett.*, 4, 20, 3513–3520, 2013.

885 Dal Maso, M., Kulmala, M., Lehtinen, K. E. J., Mäkelä, J. M., Aalto, P. P., and O’Dowd, C.:
886 Condensation and coagulation sinks and formation of nucleation mode particles in coastal and
887 boreal forest boundary layers, *J. Geophys. Res.*, 107(19D), 8097, 10.1029/2001jd001053, 2002.

888 Dal Maso, M., Kulmala, M., Riipinen, I., Wagner, R., Hussein, T., Aalto, P. P., and Lehtinen, K. E. J.:
889 Formation and growth of fresh atmospheric aerosols: eight years of aerosol size distribution data
890 from SMEAR II, Hyytiälä, Finland, *Boreal Environ. Res.*, 10, 323–336, 2005.

891 Dall’Osto, M., Querol, X., Alastuey, A., O’Dowd, C., Harrison, R. M., Wenger, J., and Gómez-
892 Moreno, F. J.: On the spatial distribution and evolution of ultrafine particles in Barcelona, *Atmos.*
893 *Chem. Phys.*, 13, 741–759, 2013.

894 Ehn, M., Thornton, J. A., Kleist, E., Sipilä, M., Junninen, H., Pullinen, I., Springer, M., Rubach, F.,
895 Tillmann, R., Lee, B., Lopez-Hilfiker, F., Andres, S., Acir, I. H., Rissanen, M., Jokinen, T.,
896 Schobesberger, S., Kangasluoma, J., Kontkanen, J., Nieminen, T., Kurten, T., Nielsen, L. B.,
897 Jørgensen, S., Kjaergaard, H. G., Canagaratna, M., Dal Maso, M., Berndt, T., Petäjä, T., Wahner,
898 A., Kerminen, V. M., Kulmala, M., Worsnop, D. R., Wildt, J., and Mentel, T. F.: A large source of
899 low-volatility secondary organic aerosol, *Nature*, 506, 476–479, 2014.

900 Gordon, H., Sengupta, K., Rap, A., Duplissy, J., Frege, C., Williamson, C., Heinritzi, M., Simon, M.,
901 Yan, C., Almeida, J., Tröstl, J., Nieminen, T., Ortega, I. K., Wagner, R., Dunne, E. M., Adamov,
902 A., Amorim, A., Bernhammer, A. K., Bianchi, F., Breitenlechner, M., Brilke, S., Chen, X., Craven,
903 J. S., Dias, A., Ehrhart, S., Fischer, L., Flagan, R. C., Franchin, A., Fuchs, C., Guida, R., Hakala, J.,
904 Hoyle, C. R., Jokinen, T., Junninen, H., Kangasluoma, J., Kim, J., Kirkby, J., Krapf, M., Kürten,
905 A., Laaksonen, A., Lehtipalo, K., Makhmutov, V., Mathot, S., Molteni, U., Monks, S. A., Onnela,
906 A., Peräkylä, O., Piel, F., Petäjä, T., Praplan, A. P., Pringle, K. J., Richards, N. A. D., Rissanen, M.
907 P., Rondo, L., Sarnela, N., Schobesberger, S., Scott, C. E., Seinfeld, J. H., Sharma, S., Sipilä, M.,
908 Steiner, G., Stozhkov, Y., Stratmann, F., Tomé, A., Virtanen, A., Vogel, A. L., Wagner, A. C.,
909 Wagner, P. E., Weingartner, E., Wimmer, D., Winkler, P. M., Ye, P., Zhang, X., Hansel, A.,
910 Dommen, J., Donahue, N. M., Worsnop, D. R., Baltensperger, U., Kulmala, M., Curtius, J., and
911 Carslaw, K. S.: Reduced anthropogenic aerosol radiative forcing caused by biogenic new particle

912 formation, *Proc. Natl. Acad. Sci. U.S.A.*, 113, 12053–12058,
913 <https://doi.org/10.1073/pnas.1602360113>, 2016.

914 Hamed, A., Korhonen, H., Sihto, S.-L., Joutsensaari, J., Järvinen, H., Petäjä, T., Arnold, F., Nieminen,
915 T., Kulmala, M., Smith, J. N., Lehtinen, K. E. J., and Laaksonen, A.: The role of relative humidity
916 in continental new particle formation. *J. Geophys. Res.*, 116, D03202, doi:10.1029/2010JD014186,
917 2011.

918 Hirsikko, A., Vakkari, V., Tiitta, P., Hatakka, J., Kerminen, V.-M., Sundström, A.-M., Beukes, J. P.,
919 Manninen, H. E., Kulmala, M., and Laakso, L.: Multiple daytime nucleation events in semi-clean
920 savannah and industrial environments in South Africa: analysis based on observations, *Atmos.*
921 *Chem. Phys.*, 13, 5523–5532, 2013.

922 Hussein, T., Puustinen, A., Aalto, P. P., Mäkelä, J. M., Hämeri, K., and Kulmala, M.: Urban aerosol
923 number size distributions, *Atmos. Chem. Phys.*, 4, 391–411, 2004.

924 Hussein, T., Martikainen, J., Junninen, H., Sogacheva, L., Wagner, R., Dal Maso, M., Riipinen, I.,
925 Aalto, P. P., and Kulmala, M.: Observation of regional new particle formation in the urban
926 atmosphere, *Tellus 60B*, 509–521, 2008.

927 Jokinen, T., Berndt, T., Makkonen, R., Kerminen, V.-M., Junninen, H., Paasonen, P., Stratmann, F.,
928 Herrmann, H., Guenther, A. B., Worsnop, D. R., Kulmala, M., Ehn, M. and Sipilä, M.: Production
929 of extremely low volatile organic compounds from biogenic emissions: Measured yields and
930 atmospheric implications, *Proc. Natl. Acad. Sci. U.S.A.*, 112, 7123–7128, 2015.

931 Kerminen, V.-M., Paramonov, M., Anttila, T., Riipinen, I., Fountoukis, C., Korhonen, H., Asmi, E.,
932 Laakso, L., Lihavainen, H., Swietlicki, E., Svenningsson, B., Asmi, A., Pandis, S. N., Kulmala, M.,
933 and Petäjä, T.: Cloud condensation nuclei production associated with atmospheric nucleation: a
934 synthesis based on existing literature and new results, *Atmos. Chem. Phys.*, 12, 12037–12059,
935 2012.

936 Kerminen, V.-M., Chen, X., Vakkari, V., Petäjä, T., Kulmala, M., and Bianchi, F.: Atmospheric new
937 particle formation and growth: review of field observations, *Environ. Res. Lett.*, 13 (2018) 103003,
938 2018.

939 Kiendler-Scharr, A., Wildt, J., Dal Maso, M., Hohaus, T., Kleist, E., Mentel, T. F., Tillmann, R.,
940 Uerlings, R., Schurr, U., and Wahner, A.: New particle formation in forests inhibited by isoprene
941 emissions, *Nature*, 461, 381–384, 2009.

942 Kirkby, J., Curtius, J., Almeida, J., Dunne, E., Duplissy, J., Ehrhart, S., Franchin, A., Gagné, S., Ickes,
943 L., Kürten, A., Kupc, A., Metzger, A., Riccobono, F., Rondo, L., Schobesberger, S.,
944 Tsagkogeorgas, G., Wimmer, D., Amorim, A., Bianchi, F., Breitenlechner, M., David, A.,
945 Dommen, J., Downard, A., Ehn, M., Flagan, R. C., Haider, S., Hansel, A., Hauser, D., Jud, W.,
946 Junninen, H., Kreissl, F., Kvashin, A., Laaksonen, A., Lehtipalo, K., Lima, J., Lovejoy, E. R.,
947 Makhutov, V., Mathot, S., Mikkilä, J., Minginette, P., Mogo, S., Nieminen, T., Onnela, A., Pereira,
948 A., Petäjä, T., Schnitzhofer, R., Seinfeld, J. H., Sipilä, M., Stozhkov, Y., Stratmann, F., Tome, A.,
949 Vanhanen, J., Viisanen Y., Vrtala, A., Wagner, P.E., Walther, H., Weingartner, E., Wex, H.,

950 Winkler, P.M., Carslaw, K. S., Worsnop, D. R., Baltensperger, U., and Kulmala, M.: The role of
951 sulfuric acid, ammonia and galactic cosmic rays in atmospheric aerosol nucleation, *Nature*, 476,
952 429–433, 2011.

953 Kirkby, J., Duplissy, J., Sengupta, K., Frege, C., Gordon, H., Williamson, C., Heinritzi, M., Simon,
954 M., Yan, C., Almeida, J., Tröstl, J., Nieminen, T., Ortega, I. K., Wagner, R., Adamov, A., Amorim,
955 A., Bernhammer, A.-K., Bianchi, F., Breitenlechner, M., Brilke, S., Chen, X., Craven, J., Dias, A.,
956 Ehrhart, S., Flagan, R. C., Franchin, A., Fuchs, C., Guida, R., Hakala, J., Hoyle, C. R., Jokinen, T.,
957 Junninen, H., Kangasluoma, J., Kim, J., Krapf, M., Kürten, A., Laaksonen, A., Lehtipalo, K.,
958 Makhmutov, V., Mathot, S., Molteni, U., Onnela, A., Peräkylä, O., Piel, F., Petäjä, T., Praplan, A.
959 P., Pringle, K., Rap, A., Richards, N. A. D., Riipinen, I., Rissanen, M. P., Rondo, L., Sarnela, N.,
960 Schobesberger, S., Scott, C. E., Seinfeld, J. H., Sipilä, M., Steiner, G., Stozhkov, Y., Stratmann, F.,
961 Tomé, A., Virtanen, A., Vogel, A. L., Wagner, A., Wagner, P. E., Weingartner, E., Wimmer, D.,
962 Winkler, P. M., Ye, P., Zhang, X., Hansel, A., Dommen, J., Donahue, N. M., Worsnop, D. R.,
963 Baltensperger, U., Kulmala, M., Carslaw, K. S., and Curtius, J.: Ion-induced nucleation of pure
964 biogenic particles, *Nature*, 533, 521–526, <https://doi.org/10.1038/nature17953>, 2016.

965 Kulmala, M., Dal Maso, M., Mäkelä, J. M., Pirjola, L., Väkevä, M., Aalto, P., Miiikkulainen, P.,
966 Hämeri, K., and O'Dowd, C. D.: On the formation, growth and composition of nucleation mode
967 particles, *Tellus B*53, 479–490, 2001.

968 Kulmala, M., Vehkamäki, H., Petäjä, T., Dal Maso, M., Lauri, A., Kerminen, V.-M., Birmili, W., and
969 McMurry, P.: Formation and growth rates of ultrafine atmospheric particles: a review of
970 observations, *J. Aerosol Sci.*, 35, 143–176, 2004.

971 Kulmala, M., Petäjä, T., Nieminen, T., Sipilä, M., Manninen, H. E., Lehtipalo, K., Dal Maso, M.,
972 Aalto, P. P., Junninen, H., Paasonen, P., Riipinen, I., Lehtinen, K. E. J., Laaksonen, A., and
973 Kerminen, V.-M.: Measurement of the nucleation of atmospheric aerosol particles, *Nat. Protoc.*, 7,
974 1651–1667, doi:10.1038/nprot.2012.091, 2012.

975 Kulmala, M., Kontkanen, J., Junninen, H., Lehtipalo, K., Manninen, H. E., Nieminen, T., Petäjä, T.,
976 Sipilä, M., Schobesberger, S., Rantala, P., Franchin, A., Jokinen, T., Järvinen, E., Äijälä, M.,
977 Kangasluoma, J., Hakala, J., Aalto, P.P., Paasonen, P., Mikkilä, J., Vanhanen, J., Aalto, J., Hakola,
978 H., Makkonen, U., Ruuskanen, T., Mauldin, R. L. III, Duplissy, J., Vehkamäki, H., Bäck, J.,
979 Kortelainen, A., Riipinen, I., Kurtén, T., Johnston, M. V., Smith, J. N., Ehn, M., Mentel, T. F.,
980 Lehtinen, K. E. J., Laaksonen, A., Kerminen, V.-M., and Worsnop, D. R.: Direct observations of
981 atmospheric aerosol nucleation, *Science*, 339, 943–946, 2013.

982 Kulmala, M., Petäjä, T., Ehn, M., Thornton, J., Sipilä, M., Worsnop, D. R., and Kerminen, V.-M.:
983 Chemistry of atmospheric nucleation: On the recent advances on precursor characterization and
984 atmospheric cluster composition in connection with atmospheric new particle formation, *Annu.
985 Rev. Phys. Chem.*, 65, 21–37, 2014.

986 Kulmala, M., Kerminen, V. M., Petäjä, T., Ding, A. J., and Wang, L.: Atmospheric gas-to-particle
987 conversion: why NPF events are observed in megacities, *Faraday Discuss.*,
988 doi:10.1039/C6FD00257A, 2017.

989 Makkonen, R., Asmi, A., Korhonen, H., Kokkola, H., Järvenoja, S., Räisänen, P., Lehtinen, K. E. J.,
990 Laaksonen, A., Kerminen, V.-M., Järvinen, H., Lohmann, U., Bennartz, R., Feichter, J., and
991 Kulmala, M.: Sensitivity of aerosol concentrations and cloud properties to nucleation and
992 secondary organic distribution in ECHAM5-HAM global circulation model, *Atmos. Chem. Phys.*,
993 9, 1747–1766, 2009.

994 Makkonen, R., Asmi, A., Kerminen, V.-M., Boy, M., Arneth, A., Hari, P., and Kulmala, M.: Air
995 pollution control and decreasing new particle formation lead to strong climate warming, *Atmos.*
996 *Chem. Phys.*, 12, 1515–1524, 2012.

997 Merikanto, J., Spracklen, D. V., Mann, G. W., Pickering, S. J., and Carslaw, K. S.: Impact of
998 nucleation on global CCN, *Atmos. Chem. Phys.*, 9, 8601–8616, 2009.

999 Metzger, A., Verheggen, B., Dommen, J., Duplissy, J., Prévôt, A. S. H., Weingartner, E., Riipinen, I.,
1000 Kulmala, M., Spracklen, D. V., Carslaw, K. S., and Baltensperger, U.: Evidence for the role of
1001 organics in aerosol particle formation under atmospheric conditions, *Proc. Natl. Acad. Sci. U. S.*
1002 *A.*, 107, 6646–6651, 2010.

1003 Németh, Z. and Salma, I.: Spatial extension of nucleating air masses in the Carpathian Basin, *Atmos.*
1004 *Chem. Phys.*, 14, 8841–8848, 2014.

1005 Németh, Z., Rosati, B., Zíková, N., Salma, I., Bozó, L., Dameto de España, C., Schwarz, J., Ždímal,
1006 V., and Wonaschütz, A.: Comparison of atmospheric new particle formation and growth events in
1007 three Central European cities, *Atmos. Environ.*, 178, 191–197, 2018.

1008 Nieminen, T., Kerminen, V.-M., Petäjä, T., Aalto, P. P., Arshinov, M., Asmi, E., Baltensperger, U.,
1009 Beddows, D. C. S., Beukes, J. P., Collins, D., Ding, A., Harrison, R. M., Henzing, B., Hooda, R.,
1010 Hu, M., Hörrak, U., Kivekäs, N., Komsaare, K., Krejčí, R., Kristensson, A., Laakso, L., Laaksonen,
1011 A., Leaitch, W. R., Lihavainen, H., Mihalopoulos, N., Németh, Z., Nie, W., O'Dowd, C., Salma, I.,
1012 Sellegri, K., Svenningsson, B., Swietlicki, E., Tunved, P., Ulevicius, V., Vakkari, V., Vana, M.,
1013 Wiedensohler, A., Wu, Z., Virtanen, A., and Kulmala, M.: Global analysis of continental boundary
1014 layer new particle formation based on long-term measurements, *Atmos. Chem. Phys.*, 18, 14737–
1015 14756, 2018.

1016 Oberdörster, G., Oberdörster, E., and Oberdörster, J.: Nanotoxicology: an emerging discipline
1017 evolving from studies of ultrafine particles, *Environ. Health Perspect.*, 113, 823–839, 2005.

1018 O'Dowd, C. D., Jimenez, J. L., Bahreini, R., Flagan, R. C., Seinfeld, J. H., Hämeri, K., Pirjola, L.,
1019 Kulmala, M., Jennings, S. G., and Hoffmann, Th.: Marine aerosol formation from biogenic iodine
1020 emissions, *Nature* 417, 632–636, 2002.

1021 Paasonen, P., Kupiainen, K., Klimont, Z., Visschedijk, A., Denier van der Gon, H. A. C., and Amann,
1022 M.: Continental anthropogenic primary particle number emissions, *Atmos. Chem. Phys.*, 16, 6823–
1023 6840, 2016.

- 1024 Paasonen, P., Peltola, M., Kontkanen, J., Junninen, H., Kerminen, V.-M., and Kulmala, M.:
1025 Comprehensive analysis of particle growth rates from nucleation mode to cloud condensation
1026 nuclei in Boreal forest, *Atmos. Chem. Phys. Discuss.*, <https://doi.org/10.5194/acp-2018-169>, in
1027 review, 2018.
- 1028 Petäjä, T., Mauldin, III, R. L., Kosciuch, E., McGrath, J., Nieminen, T., Paasonen, P., Boy, M.,
1029 Adamov, A., Kotiaho, T., and Kulmala, M.: Sulfuric acid and OH concentrations in a boreal forest
1030 site, *Atmos. Chem. Phys.*, 9, 7435–7448, 2009.
- 1031 Putaud, J.-P., Van Dingenen, R., Alastuey, A., Bauer, H., Birmili, W., Cyrus, J., Flentje, H., Fuzzi, S.,
1032 Gehrig, R., Hansson, H. C., Harrison, R. M., Herrmann, H., Hitzenberger, R., Hüglin, C., Jones,
1033 A.M., Kasper-Giebl, A., Kiss, G., Kousa, A., Kuhlbusch, T. A. J., Löschau, G., Maenhaut, W.,
1034 Molnár, A., Moreno, T., Pekkanen, J., Perrino, C., Pitz, M., Puxbaum, H., Querol, X., Rodriguez,
1035 S., Salma, I., Schwarz, J., Smolík, J., Schneider, J., Spindler, G., ten Brink, H., Turšič, J., Viana,
1036 M., Wiedensohler, and A., Raes, F.: A European Aerosol Phenomenology - 3: physical and
1037 chemical characteristics of particulate matter from 60 rural, urban, and kerbside sites across
1038 Europe, *Atmos. Environ.*, 44, 1308–1320, 2010.
- 1039 Riccobono, F., Schobesberger, S., Scott, C., Dommen, J., Ortega, I., Rondo, L., Almeida, J., Amorim,
1040 A., Bianchi, F., Breitenlechner, M., David, A., Downard, A., Dunne, E., Duplissy, J., Ehrhart, S.,
1041 Flagan, R., Franchin, A., Hansel, A., Junninen, H., Kajos, M., Keskinen, H., Kupc, A., Kurten, A.,
1042 Kvashin, A., Laaksonen, A., Lehtipalo, K., Makhmutov, V., Mathot, S., Nieminen, T., Onnela, A.,
1043 Petäjä, T., Praplan, A., Santos, F., Schallhart, S., Seinfeld, J., Sipila, M., Spracklen, D., Stozhkov,
1044 Y., Stratmann, F., Tome, A., Tsagkogeorgas, G., Vaattovaara, P., Viisanen, Y., Vrtala, A., Wagner,
1045 P., Weingartner, E., Wex, H., Wimmer, D., Carslaw, K., Curtius, J., Donahue, N., Kirkby, J.,
1046 Kulmala, M., Worsnop, D., and Baltensperger, U.: Oxidation products of biogenic emissions
1047 contribute to nucleation of atmospheric particles, *Science*, 344, 717–721, 2014.
- 1048 Riipinen, I., Pierce, J. R., Yli-Juuti, T., Nieminen, T., Häkkinen, S., Ehn, M., Junninen, H., Lehtipalo,
1049 K., Petäjä, T., Slowik, J., Chang, R., Shantz, N. C., Abbatt, J., Leaitch, W. R., Kerminen, V.-M.,
1050 Worsnop, D. R., Pandis, S. N., Donahue, N. M., and Kulmala, M.: Organic condensation: a vital
1051 link connecting aerosol formation to cloud condensation nuclei (CCN) concentrations, *Atmos.*
1052 *Chem. Phys.*, 11, 3865–3878, 2011.
- 1053 Salma, I., Borsós, T., Weidinger, T., Aalto, P., Hussein, T., Dal Maso, M., and Kulmala, M.:
1054 Production, growth and properties of ultrafine atmospheric aerosol particles in an urban
1055 environment, *Atmos. Chem. Phys.*, 11, 1339–1353, 2011.
- 1056 Salma, I., Borsós, T., Németh, Z., Weidinger, T., Aalto, T., and Kulmala, M.: Comparative study of
1057 ultrafine atmospheric aerosol within a city, *Atmos. Environ.*, 92, 154–161, 2014.
- 1058 Salma, I., Fűri, P., Németh, Z., Farkas, Á., Balásházy, I., Hofmann, W., and Farkas, Á.: Lung burden
1059 and deposition distribution of inhaled atmospheric urban ultrafine particles as the first step in their
1060 health risk assessment, *Atmos. Environ.*, 104, 39–49, 2015.

1061 Salma, I., Németh, Z., Weidinger, T., Kovács, B., and Kristóf, G.: Measurement, growth types and
1062 shrinkage of newly formed aerosol particles at an urban research platform, *Atmos. Chem. Phys.*,
1063 16, 7837–7851, 2016a.

1064 Salma, I., Németh, Z., Kerminen, V. M., Aalto, P., Nieminen, T., Weidinger, T., Molnár, Á., Imre, K.,
1065 and Kulmala, M.: Regional effect on urban atmospheric nucleation, *Atmos. Chem. Phys.*, 16,
1066 8715–8728, 2016b.

1067 Salma, I., Varga, V., and Németh, Z.: Quantification of an atmospheric nucleation and growth process
1068 as a single source of aerosol particles in a city, *Atmos. Chem. Phys.*, 17, 15007–15017, 2017.

1069 Schobesberger, S., Junninen, H., Bianchi, F., Lonn, G., Ehn, M., Lehtipalo, K., Dommen, J., Ehrhart,
1070 S., Ortega, I. K., Franchin, A., Nieminen, T., Riccobono, F., Hutterli, M., Duplissy, J., Almeida, J.,
1071 Amorim, A., Breitenlechner, M., Downard, A. J., Dunne, E. M., Flagan, R. C., Kajos, M.,
1072 Keskinen, H., Kirkby, J., Kupc, A., Kurten, A., Kurten, T., Laaksonen, A., Mathot, S., Onnela, A.,
1073 Praplan, A. P., Rondo, L., Santos, F. D., Schallhart, S., Schnitzhofer, R., Sipilä, M., Tome, A.,
1074 Tsagkogeorgas, G., Vehkamäki, H., Wimmer, D., Baltensperger, U., Carslaw, K. S., Curtius, J.,
1075 Hansel, A., Petäjä, T., Kulmala, M., Donahue, N. M., and Worsnop, D. R.: Molecular
1076 understanding of atmospheric particle formation from sulfuric acid and large oxidized organic
1077 molecules, *Proc. Natl. Acad. Sci. U.S.A.*, 110, 17223–17228, 10.1073/pnas.1306973110, 2013.

1078 Sihto, S.-L., Mikkilä, J., Vanhanen, J., Ehn, M., Liao, L., Lehtipalo, K., Aalto, P. P., Duplissy, J.,
1079 Petäjä, T., Kerminen, V.-M., Boy, M., and Kulmala, M.: Seasonal variation of CCN concentrations
1080 and aerosol activation properties in boreal forest, *Atmos. Chem. Phys.*, 11, 13269–13285, 2011.

1081 Sipilä, M., Berndt, T., Petäjä, T., Brus, D., Vanhanen, J., Stratmann, F., Patokoski, J., Mauldin, R. L.
1082 3rd, Hyvärinen, A. P., Lihavainen, H., and Kulmala, M.: The role of sulfuric acid in atmospheric
1083 nucleation, *Science*, 327(5970), 1243–6. doi: 10.1126/science.1180315, 2010.

1084 Spracklen, D. V., Carslaw, K. S., Merikanto, J., Mann, G. W., Reddington, C. L., Pickering, S., Ogren,
1085 J. A., Andrews, E., Baltensperger, U., Weingartner, E., Boy, M., Kulmala, M., Laakso, L.,
1086 Lihavainen, H., Kivekäs, N., Komppula, M., Mihalopoulos, N., Kouvarakis, G., Jennings, S. G.,
1087 O'Dowd, C., Birmili, W., Wiedensohler, A., Weller, R., Gras, J., Laj, P., Sellegri, K., Bonn, B.,
1088 Krejčí, R., Laaksonen, A., Hamed, A., Minikin, A., Harrison, R. M., Talbot, R., and Sun, J.: The
1089 contribution of boundary layer nucleation events to total particle concentrations on regional and
1090 global scales, *Atmos. Chem. Phys.*, 6, 5631–5648, 2006.

1091 Sun, J., Birmili, W., Hermann, M., Tuch, T., Weinhold, K., Spindler, G., Schladitz, A., Bastian, S.,
1092 Löschau, G., Cyrys, J., Gu, J., Flentje, H., Briel, B., Asbach, C., Kaminski, H., Ries, L., Sohmer,
1093 R., Gerwig, H., Wirtz, K., Meinhardt, F., Schwerin, A., Bath, O., Ma, N., and Wiedensohler, A.:
1094 Variability of Black Carbon mass concentrations, sub-micrometer particle number concentrations
1095 and size distributions: Results of the German Ultrafine Aerosol Network ranging from city street to
1096 high Alpine locations, *Atmos. Environ.*, 202, 256–268, 2019.

1097 Tröstl, J., Chuang, W. K., Gordon, H., Heinritzi, M., Yan, C., Molteni, U., Ahlm, L., Frege, C.,
1098 Bianchi, F., Wagner, R., Simon, M., Lehtipalo, K., Williamson, C., Craven, J. S., Duplissy, J.,

1099 Adamov, A., Almeida, J., Bernhammer, A. K., Breitenlechner, M., Brilke, S., Dias, A., Ehrhart, S.,
1100 Flagan, R. C., Franchin, A., Fuchs, C., Guida, R., Gysel, M., Hansel, A., Hoyle, C. R., Jokinen, T.,
1101 Junninen, H., Kangasluoma, J., Keskinen, H., Kim, J., Krapf, M., Kürten, A., Laaksonen, A.,
1102 Lawler, M., Leiminger, M., Mathot, S., Möhler, O., Nieminen, T., Onnela, A., Petäjä, T., Piel, F.
1103 M., Miettinen, P., Rissanen, M. P., Rondo, L., Sarnela, N., Schobesberger, S., Sengupta, K., Sipilä,
1104 M., Smith, J. N., Steiner, G., Tomè, A., Virtanen, A., Wagner, A. C., Weingartner, E., Wimmer, D.,
1105 Winkler, P. M., Ye, P. L., Carslaw, K. S., Curtius, J., Dommen, J., Kirkby, J., Kulmala, M.,
1106 Riipinen, I., Worsnop, D. R., Donahue, N. M., and Baltensperger, U.: The role of low-volatility
1107 organic compounds in initial particle growth in the atmosphere, *Nature*, 533, 527,
1108 10.1038/nature18271, 2016.

1109 Vakkari, V., Tiitta, P., Jaars, K., Croteau, P., Beukes, J. P., Josipovic, M., Kerminen, V.-M., Kulmala,
1110 M., Venter, A. D., van Zyl, P. G., Worsnop, D. R., and Laakso, L.: Reevaluating the contribution of
1111 sulfuric acid and the origin of organic compounds in atmospheric nanoparticle growth, *Geophys.*
1112 *Res. Lett.*, 42, 10486–10493, 2015.

1113 Vuollekoski, H., Sihto, S.-L., Kerminen, V.-M., Kulmala, M., and Lehtinen, K. E. J.: A numerical
1114 comparison of different methods for determining the particle formation rate, *Atmos. Chem. Phys.*,
1115 12, 2289–2295, 2012.

1116 Wehner, B., Wiedensohler, A., Tuch, T. M., Wu, Z. J., Hu, M., Slanina, J., and Kiang, C. S.:
1117 Variability of the aerosol number size distribution in Beijing, China: new particle formation, dust
1118 storms, and high continental background, *Geophys. Res. Lett.*, 31, L22108, 2004.

1119 Wiedensohler, A., Cheng, Y. F., Nowak, A., Wehner, B., Achtert, P., Berghof, M., Birmili, W., Wu, Z.
1120 J., Hu, M., Zhu, T., Takegawa, N., Kita, K., Kondo, Y., Lou, S. R., Hofzumahaus, A., Holland, F.,
1121 Wahner, A., Gunthe, S. S., Rose, D., Su, H., and Pöschl, U.: Mobility particle size spectrometers:
1122 harmonization of technical standards and data structure to facilitate high quality long-term
1123 observations of atmospheric particle number size distributions, *Atmos. Meas. Tech.*, 5, 657–685,
1124 2012.

1125 Woo, K. S., Chen, D. R., Pui, D. Y. H., and McMurry, P. H.: Measurement of Atlanta aerosol size
1126 distributions: observations of ultrafine particle events, *Aerosol Sci. Technol.*, 34, 75–87, 2001.

1127 Xiao, S., Wang, M. Y., Yao, L., Kulmala, M., Zhou, B., Yang, X., Chen, J. M., Wang, D. F., Fu, Q.
1128 Y., Worsnop, D. R., and Wang, L.: Strong atmospheric new particle formation in winter in urban
1129 Shanghai, China, *Atmos. Chem. Phys.*, 15, 1769–1781, 2015.

1130 Yli-Juuti, T., Riipinen, I., Aalto, P. P., Nieminen, T., Maenhaut, W., Janssens, I. A., Claeys, M.,
1131 Salma, I., Ocskay, R., Hoffer, A., Imre, K., and Kulmala, M.: Characteristics of new particle
1132 formation events and cluster ions at K-pusztá, Hungary. *Boreal Environ. Res.*, 14, 683–698, 2009.

1133 Zhang, R., Wang, G., Guo, S., Zamora, M. L., Ying, Q., Lin, Y., Wang, W., Hu, M., and Wang, Y.:
1134 Formation of urban fine particulate matter, *Chem. Rev.*, 115, 3803–3855, 2015.